

1 **Modeling of PAHs From Global to Regional Scales:** 2 **Model Development (IAP-AACM_PAH v1.0) and** 3 **Investigation of Health Risks in 2013 and 2018 in China**

4 Zichen Wu^{1,2,3}, Xueshun Chen^{1,2,3*}, Zifa Wang^{1,2,3*}, Huansheng Chen^{1,2,3}, Zhe
5 Wang^{1,2,3}, Qing Mu⁴, Lin Wu^{1,2,3}, Wending Wang^{1,2,3}, Xiao Tang^{1,2,3}, Jie Li^{1,2,3}, Ying
6 Li^{1,2,3}, Qizhong Wu⁵, Yang Wang^{3,6}, Zhiyin Zou^{1,2,3}, Zijian Jiang^{1,2,3}

7 ¹ State Key Laboratory of Atmospheric Boundary Layer Physics and Atmospheric Chemistry, Institute
8 of Atmospheric Physics, Chinese Academy of Sciences, Beijing 100029, China

9 ² Key Laboratory of Atmospheric Environment and Extreme Meteorology, Institute of Atmospheric
10 Physics, Chinese Academy of Sciences, Beijing 100029, China

11 ³ University of Chinese Academy of Sciences, Beijing 100049, China

12 ⁴ Department of Health and Environmental Sciences, School of Science, Xi'an Jiaotong-Liverpool
13 University, Suzhou 215123, China

14 ⁵ Beijing Normal University, Beijing 100875, China

15 ⁶ Research Center for Eco-Environmental Sciences, Chinese Academy of Sciences, Beijing 100085,
16 China

17 *Correspondence to:* Xueshun Chen (chenxsh@mail.iap.ac.cn) and Zifa Wang (zifawang@mail.iap.ac.cn)

18 **Abstract.** Polycyclic aromatic hydrocarbons (PAHs) significantly impact human health due to their
19 persistence, toxicity, and potential carcinogenicity. Their global distribution and regional changes caused
20 by emission changes, especially over areas in developing countries, remain to be understood along with
21 their health impacts. This study implemented a PAH module in the global-regional nested Atmospheric
22 Aerosol and Chemistry Model (IAP-AACM) to investigate the global distribution of PAHs and the
23 change in their health risks from 2013 to 2018 in China. An evaluation against observations showed that
24 the model could capture well the spatial distribution and seasonal variation of Benzo[a]pyrene (BaP), the
25 typical indicator species of PAHs. At a global scale, the annual mean concentrations are highest in China,
26 followed by Europe and India, with high values exceeding the target values of 1 ng m⁻³ over some areas.
27 Compared with 2013, the concentration of BaP in China decreased in 2018 due to emission reductions,
28 whereas it increased in India and Southern Africa. However, the decline is much smaller than for PM_{2.5}
29 during the same period. The concentration of BaP decreased by 8.5% in Beijing-Tianjin-Hebei (BTH)
30 and 9.4% in the Yangtze River Delta (YRD). It even increased over areas in the Sichuan Basin due to
31 changes in meteorological conditions. The total incremental lifetime cancer risk (ILCR) posed by BaP

32 only showed a slight decrease in 2018 and the population in East China still faced significant potential
33 health risks. The results indicate that strict additional control measures should be taken to reduce the
34 pollution and health risks of PAHs effectively. The study also highlights the importance of considering
35 changes in meteorological conditions when evaluating emission changes from concentration monitoring.

36 **1 Introduction**

37 Polycyclic aromatic hydrocarbons (PAHs) are aromatic compounds with two or more aromatic rings.
38 PAHs have been categorized as persistent organic pollutants (POPs) by the United Nations Economic
39 Commission for Europe's (UNECE's) Convention on Long-Range Transboundary Air Pollution
40 (CLRTAP) (Friedman and Selin, 2012), and they are widely distributed in the environment through
41 atmospheric transport. PAHs have attracted significant attention in environmental research and risk
42 assessment due to their persistence, toxicity, and potential carcinogenicity (Chen and Liao, 2006; Shen
43 et al., 2014). These compounds are generated from both natural and anthropogenic sources (Haritash and
44 Kaushik, 2009). Volcanic eruption, forest, and prairie fire are the major natural sources of atmospheric
45 PAHs (Baek et al., 1991). Anthropogenic sources are the most important source of PAHs, including
46 incomplete combustion of fossil fuels and biomass (Li et al., 2022; Ravindra et al., 2008).

47 Understanding the sources, distribution, and fate of PAHs is crucial for assessing their impacts on
48 human health and the environment. Upon emission into the atmosphere, PAHs are redistributed by gas-
49 particulate partitioning, gaseous-phase reactions, heterogeneous reactions, air-soil exchange, and wet/dry
50 deposition during long-range transport (LRT, Inomata et al., 2013). Monitoring is the most commonly
51 used way to investigate the concentration of PAHs in the atmosphere. Due to the high costs of observation
52 and technical limitations, it is difficult to conduct a long-term and broad regional analysis through
53 monitoring (Zhen, 2023). Up to now, there are few continuous observations over the major continents at
54 the same time (Dong et al., 2023). A transport model is an effective tool to simulate the distribution of
55 PAHs and their LRT, which can greatly enhance our understanding of the distribution of PAHs on a
56 regional and global scale (Byun and Schere, 2006; Wang et al., 2021).

57 As recently outlined by Galarnau et al. (2014), several numerical modeling studies have been
58 reported in the literature. The models that can simulate PAHs include but are not limited to the following
59 examples, GEOS-Chem (Friedman et al., 2014; Friedman and Selin, 2012), ECHAM5 (Lammel and

60 Sehili, 2007; Lammel et al., 2009; Lammel et al., 2015; Octaviani et al., 2019), CAM5 (Lou et al., 2023;
61 Shrivastava et al., 2017), and MOZART-4 (Shen et al., 2014). The horizontal resolutions of these reported
62 models are primarily at $4^{\circ} \times 5^{\circ}$ and $2.8^{\circ} \times 2.8^{\circ}$. Shen et al. (2014) simulated the transport of
63 Benzo[a]pyrene (BaP), one of the most toxic and highly carcinogenic PAHs, in the global troposphere
64 based on MOZART-4, and they showed that the model resolution was crucial for the health risks
65 assessment. Lammel et al. (2015) demonstrated the significant impact of gas-particle partitioning
66 mechanisms on the atmospheric lifetime, compartment distributions, and LRT of PAHs. The regional
67 modeling studies focusing on Europe, East Asia, and North America have also been reported, with
68 horizontal resolutions ranging mainly from $54 \text{ km} \times 54 \text{ km}$ to $24 \text{ km} \times 24 \text{ km}$ (CMAQ (Aulinger et al.,
69 2009; Aulinger et al., 2007; Bieser et al., 2012; San José et al., 2013; Efstathiou et al., 2016), WRF-Chem
70 (Mu et al., 2018), AURAMS (Galarneau et al., 2014), and CanMETO (Zhang et al., 2011a; Zhang et al.,
71 2011b; Zhang et al., 2009)). Efstathiou et al. (2016) showed that considering absorption and adsorption
72 processes can better capture the concentration levels and seasonal variations of BaP. In recent years, the
73 effect of the heterogeneous reaction process of PAHs on transportation has also been studied. Mu et al.
74 (2018) developed a new kinetic scheme describing the effects of temperature and humidity on the organic
75 aerosol coating of BaP and BaP reaction rate. They found that low temperature and low humidity can
76 significantly increase the lifetime of BaP and enhance its LRT capacity.

77 However, the resolutions and spatial range differed greatly between these models. Most of the
78 models are either global or regional. There is a lack of simulation studies focusing on both global and
79 key regions, making it difficult to investigate a specific focus in a global background in a consistent
80 manner. Additionally, the resolution of most global models is low, which will further affect the health
81 risk assessment of PAHs. Furthermore, the up-to-date mechanisms (gas-particle partitioning,
82 heterogeneous reaction, and air-soil exchange) established for PAHs simulations are not considered in
83 earlier modeling studies.

84 China is one of the largest PAH-emitting countries in the world (Inomata et al., 2012; Zhang and
85 Tao, 2009). High concentrations of BaP have been reported (Bieser et al., 2012; Liu et al., 2014;
86 Shrivastava et al., 2017; Su et al., 2023). Over the polluted regions in eastern China, annual
87 concentrations of BaP exceeded 1 ng m^{-3} , the target values proposed in the European Union (EU) and
88 China. To improve air quality and protect public health, the State Council of China promulgated “the

89 Action Plan on Air Pollution Prevention and Control” (the Action Plan) in 2013. **This Action Plan**
90 **established many effective emission reduction and energy-saving policies, such as strengthening**
91 **industrial emission standards, eliminating outdated polluting industries, upgrading industrial**
92 **boilers, and developing clean fuels in the residential sector.** Since then, many studies have investigated
93 the changes in concentration levels and health risks of conventional pollutants, such as PM_{2.5} (Feng et
94 al., 2019; Wang et al., 2018; Zhang et al., 2019; Zhu et al., 2021; Wang et al., 2019). Wang et al. (2019)
95 pointed out that the annual average concentrations of PM_{2.5} in the Beijing-Tianjin-Hebei (BTH), the
96 Yangtze River Delta (YRD), and the Pearl River Delta (PRD) all decreased by more than 27% in 2017,
97 indicating that the control measures have achieved remarkable effects and the air quality has been
98 significantly improved. However, for non-conventional pollutants, such as BaP and other PAHs, their
99 concentration changes due to emission reduction in China after implementing of policies have not been
100 quantified. The changes in health risks and the benefits from control measures were not yet assessed.

101 Considering the aforementioned, we simulated PAHs from global to regional scales by coupling the
102 key physical and chemical modules associated with PAHs in a global-regional nested atmospheric
103 transport model. In particular, newly established parametrizations of gas-particle partitioning and
104 heterogeneous reaction were incorporated into the model. Then the changes in global concentration and
105 health risks of BaP over China were quantified based on model evaluation against a collected observation
106 dataset. The study can advance our understanding of global PAHs distribution and regional health risks
107 and their responses to emission change. The paper is arranged as follows: Section 2 briefly describes the
108 host model (IAP-AACM), the physical and chemical modules related to PAHs, and the method of
109 assessing health risks. Section 3 presents the configuration of the model and the observations used in the
110 evaluation. Section 4 shows the global and regional distributions of BaP concentrations and analyzes the
111 health risks associated with BaP in China. Section 5 discusses the uncertainty of the model. In Sect. 6,
112 the main conclusions are summarized.

113 **2 Model description and development**

114 **2.1 Description of host model**

115 The model used in this study is the Atmospheric Aerosol and Chemistry Model developed by the
116 Institute of Atmospheric Physics, Chinese Academy of Sciences (IAP-AACM) (Wei et al., 2019), which

117 was developed based on the Global Nested Air Quality Prediction Modeling System (GNAQPMS, Chen
118 et al., 2015; Wang et al., 2001). IAP-AACM is a 3-D Eulerian transport model that uses a multi-scale
119 domain-nesting approach to simulate atmospheric chemistry and aerosol processes from global to
120 regional scales. As recently described by Chen et al. (2015), compared with the traditional multi-scale
121 modeling methods (Seigneur et al., 2001), the online nesting method uses the same parameters in the
122 global and regional domains, which avoids uncertainties caused by different boundary conditions, and it
123 also provides boundary conditions at higher time resolution (Zhang et al., 2012b; Chen et al., 2015), thus
124 improving the performance of the model at the regional scale.

125 This model includes emission, horizontal and vertical advection (Walcek and Aleksic, 1998),
126 diffusion (Byun and Dennis, 1995), dry deposition (Zhang et al., 2003), gaseous chemistry (CBM-Z,
127 Carbon Bond Mechanism version Z, Zaveri and Peters, 1999), heterogeneous chemistry (Li et al., 2012),
128 aqueous reactions in clouds, and wet scavenging (Stockwell et al., 1990). It has been successfully and
129 widely applied to simulate the spatial-temporal distribution characteristics of gaseous pollutants, aerosol
130 components, and the long-distance transportation of mercury (Chen et al., 2015; Chen et al., 2014; Wei
131 et al., 2019; Ye et al., 2021; Du et al., 2019). In addition, advanced particle microphysics (APM) has been
132 incorporated to simulate new particle formation processes and predict the particle number concentrations
133 at global and regional scales (Chen et al., 2021).

134 **2.2 Development of the PAH module**

135 The PAH processes in the IAP-AACM model include gaseous-phase reaction, heterogeneous
136 reaction, gas-particle partitioning, air-soil exchange, dry deposition, and wet scavenging. The simulated
137 species include BaP, Benzo[b]fluorathene (BbF), Benzo[k]fluorathene (BkF), and Indeno[1,2,3-
138 cd]pyrene (IcdP) in the gas and particulate phases (Wu et al., 2024). In this study, we mainly focus on
139 BaP due to its highly carcinogenic nature and the relatively rich observations.

140 **2.2.1 Gaseous-phase reactions**

141 PAHs are degraded through reactions with various atmospheric oxidants such as hydroxyl radical
142 (OH), nitrate radical (NO₃), and ozone (O₃) in the troposphere (Lammel and Schili, 2007). Among these
143 oxidants, the reactions with OH are considered to be the most important pathway for the removal of
144 PAHs. The nighttime reaction of PAHs with NO₃ is also important in the atmosphere (Keyte et al., 2013).

145 Therefore, reactions of gaseous-phase BaP with OH, NO₃, and O₃ are all considered in the model. The
 146 second-order rate coefficients are 5.0×10⁻¹¹, 5.4×10⁻¹¹, and 2.6×10⁻¹⁷ cm³ molecules⁻¹ s⁻¹, respectively
 147 (Inomata et al., 2013; Finlayson-Pitts and Pitts, 2000; Klöpffer et al., 2007).

148 2.2.2 Heterogeneous reaction

149 In the case of BaP, the heterogeneous reaction with O₃ is considered to be the dominant loss
 150 (Finlayson - Pitts and Pitts, 2000; Efstathiou et al., 2016). Studies have shown that the process of
 151 heterogeneous reaction can be well described by the Langmuir-Hinshelwood mechanism (Kahan et al.,
 152 2006; Kwamena et al., 2007), in which BaP is adsorbed to the surface while the O₃ is in phase equilibrium.
 153 The first-order reaction rate coefficient k (s⁻¹) of the Langmuir-Hinshelwood mechanism is as follows:

$$k = \frac{k_{max}K_{O_3}[O_3]}{1 + K_{O_3}[O_3]} \quad (1)$$

$$\frac{\partial C}{\partial t} = -K_{O_3}[O_3] \quad (2)$$

154 Where k_{max} is the maximum rate coefficient, and the value is 0.060±0.018 s⁻¹. $[O_3]$ is the
 155 concentration of O₃ (mol cm⁻³). K_{O_3} is the O₃ to surface equilibrium constant (0.028±0.014×10⁻¹³ cm³).

156 In addition, we incorporated a more detailed parameterization (ROI-T) developed by Mu et al. (2018)
 157 based on the Langmuir-Hinshelwood mechanism. The scheme emphasizes the importance of
 158 representing the dependence of degradation on temperature and humidity, when coated by organic
 159 aerosols The first-order reaction rate coefficient k (s⁻¹) is given by Eq. (3).

$$k = base + \frac{max - base}{1 + (\frac{xhalf}{[O_3]})^{rate}} \quad (3)$$

160 Where $base$, max , $rate$, and $xhalf$ are all the parameterizations of the heterogeneous reaction,
 161 with specific values shown in Mu et al. (2018). In our study, we coupled these two parameterizations as
 162 two options for O₃ degradation by heterogeneous reaction in IAP-AACM. The model results using these
 163 two schemes were compared to analyze the influence of heterogeneous reaction schemes on BaP
 164 concentration. The ROI-T scheme was used as the default in this study.

165 2.2.3 Gas-particle partitioning

166 The partition of compounds between the gas and particulate phases is parameterized with the gas-
 167 particle partitioning coefficient (K_p , m³ μg⁻¹) (Harner and Bidleman, 1998):

$$K_p = \left(\frac{[PAH]_p}{[TSP]} \right) / [PAH]_g \quad (4)$$

168 Where $[PAH]_g$ and $[PAH]_p$ are the concentrations of PAHs in the gas and particulate phase
 169 ($\mu\text{g m}^{-3}$), and $[TSP]$ is the concentration of total suspended particles (TSP, $\mu\text{g m}^{-3}$) in the atmosphere
 170 ($\mu\text{g m}^{-3}$).

171 Adsorption onto black carbon (BC) and absorption into aerosol organic matter (OM) are two
 172 important mechanisms of gas-particle partitioning (Odabasi et al., 2006). Therefore, we use the gas-
 173 particle partition coefficient equation to represent these two mechanisms, which was derived by Dachs
 174 and Eisenreich, 2000:

$$K_p = \left[\frac{(f_{OM} MW_{OCT} \delta_{OCT}) K_{OA}}{(\rho_{OCT} MW_{OM} \delta_{OM} 10^{12})} \right] + \left[\left(\frac{f_{BC} a_{BC} K_{SA}}{a_{AC} 10^{12}} \right) \right] \quad (5)$$

175 Where MW_{OCT} and MW_{OM} are the mean molecular weights of octanol and OM phase (g mol^{-1}),
 176 δ_{OCT} and δ_{OM} are the activity coefficient of the absorbing compound in octanol and OM phase,
 177 respectively. f_{OM} and f_{BC} are the mass fractions of OM phase on TSP and the BC in the aerosol. ρ_{OCT}
 178 is the density of octanol (0.820 kg L^{-1}). a_{BC} and a_{AC} are the specific surface areas of BC ($62.7 \text{ m}^2 \text{ g}^{-1}$,
 179 Jonker and Koelmans, 2002) and activated carbon (AC), respectively. In this study, we use the same
 180 assumption as Odabasi et al. (2006) ($MW_{OCT}/MW_{OM} = 1$, $\delta_{OCT}/\delta_{OM} = 1$, and $a_{BC}/a_{AC} = 1$).

$$\log K_{OA} = A + B/(T) \quad (6)$$

181 Where K_{OA} is the octanol-air partitioning coefficient (temperature dependent). T is the
 182 temperature (K). The values of A and B are 5382 and -6.5, respectively (Odabasi et al., 2006).

$$\log P_L = m_L(T)^{-1} + b_L \quad (7)$$

$$\log K_{SA} = -0.85 \log P_L + 8.94 - \log \left(\frac{998}{a_{BC}} \right) \quad (8)$$

183 Where P_L is the supercooled liquid vapor pressure (Pa). The values of b_L and m_L are 12.59 and
 184 -5252, respectively (Dachs and Eisenreich, 2000). K_{SA} is the soot-air partitioning coefficient (L kg^{-1}),
 185 which is a function of P_L and a_{BC} (van Noort, 2003).

186 2.2.4 Air-soil exchange

187 The semi-volatility and persistence of PAHs allow them to dynamically exchange between the
 188 atmosphere and soil by deposition and re-volatilization from ground surfaces (Semeena and Lammel,
 189 2005). These processes can affect the distribution and long-distance transport of PAHs in the environment.
 190 As described by Hansen et al. (2004), air-soil exchange is parameterized following Strand and Hov

191 (1996), which is based on Jury et al. (1983). Here, soil (standard soil) is considered to be a homogeneous
 192 layer of thickness $z_s = 0.15$ m, and standard values and chemical properties are provided by Jury et al.
 193 (1983) (Table S1). The differential equation for the change of concentrations in soil and air can be
 194 expressed by Eq. (9) and Eq. (10):

$$\frac{\partial c_s}{\partial t} = \frac{1}{z_s} (F_{exc,soil} + F_{wet}) - k_{soil} c_s \quad (9)$$

$$\frac{\partial c_a}{\partial t} = -\frac{1}{z_a} F_{exc,soil} \quad (10)$$

195 Where C_a and C_s are the concentrations of PAHs in the atmosphere and soil, respectively. The z_a
 196 is the lowest atmospheric layer depths (m), F_{wet} is the wet deposition flux ($\text{mol s}^{-1} \text{m}^{-2}$). k_{soil} is the
 197 degradation rate in soil, which is estimated to be $2.2 \times 10^{-8} \text{ s}^{-1}$ (Finlayson - Pitts and Pitts, 2000; Klöpffer
 198 et al., 2007; Lammel et al., 2009). The air–soil exchange flux ($F_{exc,soil}$) is given by Eq. (11):

$$F_{exc,soil} = K_{a/s} (c_a - \frac{c_s}{K_{soil-air}}) \quad (11)$$

199 $K_{soil-air}$ is the partitioning coefficient between soil and air, which is given by Karickhoff (1981):

$$K_{soil-air} = 4.11 \times 10^{-4} \times \rho_s f_{oc} K_{OA} \quad (12)$$

200 Where f_{oc} is the fraction of OC in soil and 4.11×10^{-4} is a constant with units of $\text{m}^3 \text{kg}^{-1}$. ρ_s is the
 201 density of soil. $K_{a/s}$ is the overall exchange velocity (m s^{-1}), which can be estimated by Eq. (13) (Strand
 202 and Hov, 1996):

$$K_{a/s} = \frac{D_G^{air} a^{10/3} (1-l-a)^{-2} + D_L^{water} l^{10/3} K_{WA} (1-l-a)^{-2}}{z_s/2} \quad (13)$$

203 Where D_G^{air} and D_L^{water} are the air and liquid diffusion coefficient ($\text{m}^2 \text{s}^{-1}$), respectively. K_{WA} is
 204 the water-air partitioning coefficient. The differential equation is solved the ODEPACK
 205 (<https://github.com/jacobwilliams/odepack>).

206 2.2.5 Dry and wet deposition

207 PAHs can be removed from the atmosphere and enter terrestrial ecosystems through dry and wet
 208 deposition (Cao et al., 2021). Dry deposition and wet scavenging have been included in IAP-AACM. For
 209 the gaseous species of PAHs, their wet scavenging is assumed to be the same as xylene in the CBMZ
 210 mechanism, which is also an aromatic hydrocarbon like BaP; for the PAHs in the particle phase, these
 211 two processes are treated similarly to that of organic aerosol.

212 **2.3 Risk assessment**

213 The incremental lifetime cancer risk (ILCR) is widely used to calculate the risk of human exposure
214 to PAHs (Nam et al., 2021). The carcinogenic risk of PAHs to humans through different exposure routes
215 was calculated based on the health risk evaluation model proposed by the U.S. Environmental Protection
216 Agency (EPA) (Smith et al., 1999).

217 The national population data **at 1 km × 1 km (at the Equator) resolution** in 2013 and 2018 were
218 obtained from the LandScan (Oak Ridge National Laboratory; database can be accessed via:
219 <https://landscan.ornl.gov>, last access: 20 January 2024) and re-gridded to 1° × 1° and 0.33° × 0.33° to
220 match the model resolution.

221 **2.3.1 Daily exposure dose**

222 Dermal contact and inhalation are regarded as the major routes of human exposure to BaP (Li et al.,
223 2010; Ma et al., 2020; Zhang et al., 2016). In this study, the health risk for the entire population and three
224 groups (adult women, adult men, and children) are calculated. The daily exposure dose (ADD) to PAHs
225 through the two exposure routes is calculated as follows:

$$ADD_{der} = \frac{C \times SA \times ABS \times AF \times EF \times ED}{AT \times BW} \quad (14)$$

$$ADD_{inh} = \frac{C \times IR \times EF \times ED}{AT \times BW} \quad (15)$$

226 Where ADD_{der} and ADD_{inh} are the average daily exposure dose that enters the body through the
227 dermal contact and inhalation, respectively ($\text{ng kg}^{-1} \text{ day}^{-1}$), C is the concentration of PAHs (ng m^{-3}). IR
228 is the inhalation rate ($\text{m}^3 \text{ d}^{-1}$). **AF is the dermal adherence rate ($\text{mg cm}^{-2} \text{ d}^{-1}$).** EF and ED are the
229 exposure duration (d a^{-1}) and period (a), respectively. BW is the body weight (kg). SA is the skin
230 exposed surface area (cm^2). ABS is the skin absorption factor. AT is the average exposure time (d).
231 The values are shown in Table S2.

232 **2.3.2. Incremental lifetime cancer risk (ILCR)**

233 The ILCR was calculated based on the ADD:

$$ILCR_{der} = ADD_{der} \times SFO_{der} \times CF \quad (16)$$

$$ILCR_{inh} = ADD_{inh} \times SFO_{inh} \times CF \quad (17)$$

$$TILCR = ILCR_{der} + ILCR_{inh} \quad (18)$$

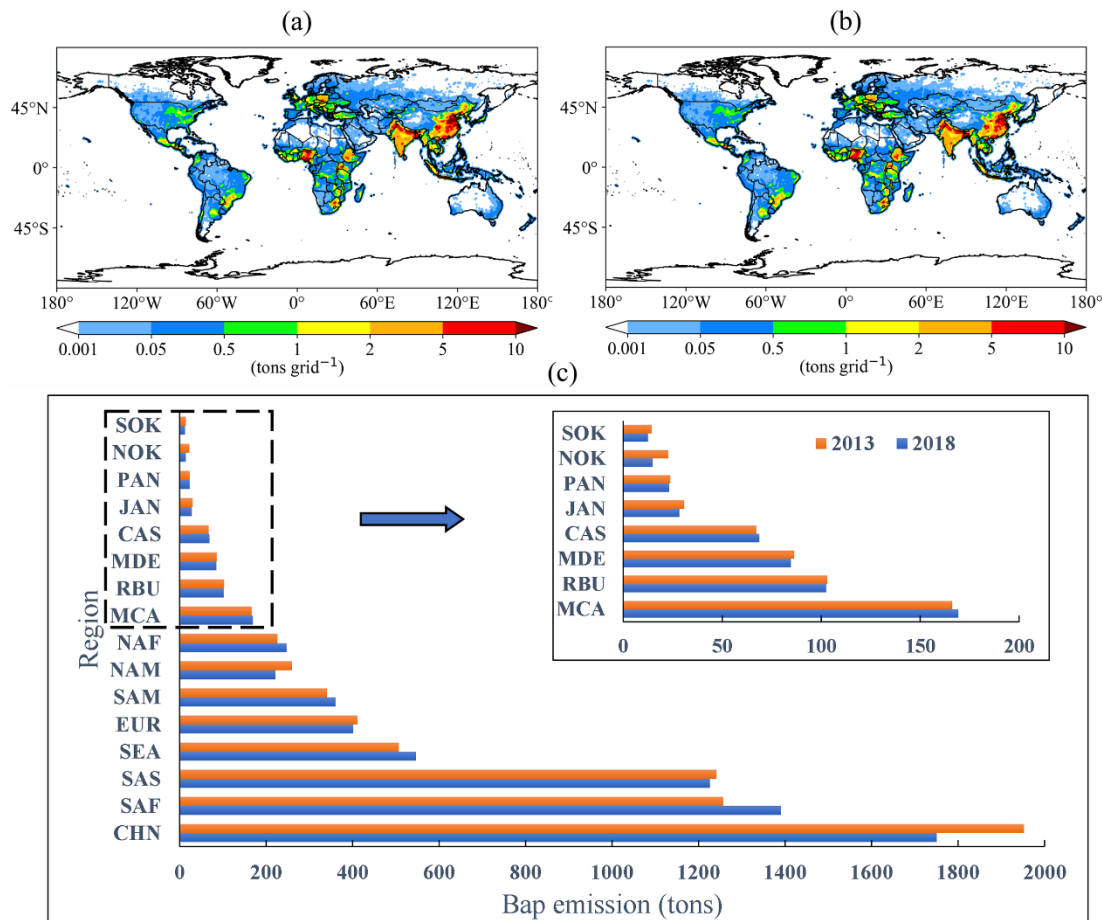
234 Where $ILCR_{der}$ and $ILCR_{inh}$ are lifetime cancer risks through the dermal contact and inhalation,
235 respectively. $TILCR$ is the total lifetime cancer risk of exposure through the two pathways. SFO is a
236 cancer slope factor (kg day mg^{-1}) and CF is the conversion factor. The values are shown in Table S2.
237 For carcinogen, an $ILCR$ less than 1×10^{-6} indicates negligible cancer risk, an $ILCR$ between 1×10^{-6}
238 and 1×10^{-4} indicates potential cancer risk, and an $ILCR$ larger than 1×10^{-4} indicates high potential
239 cancer risk.

240 3 Experiments setup and observation data

241 3.1 Experiments setup

242 In this study, we used two nested domains covering the whole globe and East Asia as shown in Fig.
243 S1. The horizontal resolutions are $1^\circ \times 1^\circ$ and $0.33^\circ \times 0.33^\circ$, respectively. A total of 20 vertical layers are
244 used in IAP-AACM. The first layer of the model is approximately 50 m deep and the top layer extends
245 to 20 km. The simulation results from January 1st to December 31st 2013 and from January 1st to
246 December 31st 2018 were used for analysis. Each simulation had a one-month spin-up before January 1st
247 to reduce the influence of initial conditions. The global version of the Weather Research and Forecasting
248 model (WRF, version 3.7.1) (Zhang et al., 2012a; Skamarock et al., 2008) provides the meteorological
249 fields to drive the IAP-AACM. The initial and boundary conditions of the global WRF were produced
250 by Final Analysis data (FNL) from the National Centers for Environmental Prediction (NCEP).

251 The emission inventory of BaP in 2013 and 2018 was derived from the Emissions Database for
252 Global Atmospheric Research (EDGAR, Crippa et al., 2020, available from
253 https://edgar.jrc.ec.europa.eu/dataset_pop60#sources, last access: 15 December 2023). We mainly
254 analyzed the results using EDGAR emission, which mainly includes anthropogenic sources such as
255 power, transportation, industrial, agricultural, and energy for buildings. An additional simulation for 2013
256 using the emission inventory developed by the research group of Peking University (PKU)
257 (<http://inventory.pku.edu.cn>, last access: 10 February 2023) was used to investigate the uncertainties
258 from emissions. The resolution of both emission inventories is $0.1^\circ \times 0.1^\circ$. Therefore, we re-gridded the
259 emissions inventories to match the model grids at $1^\circ \times 1^\circ$ and $0.33^\circ \times 0.33^\circ$ resolution.



260
 261 **Figure 1. Spatial distributions of total emissions of BaP in (a) 2013 and (b) 2018 based on the EDGAR**
 262 **inventory. (c) BaP emissions for 16 regions (except oceans, Arctic, and Antarctic) in 2013 and 2018.**

263 The global total emissions of BaP in 2013 and 2018 are shown in Fig. 1a and 1b, respectively. The
 264 annual emissions in different regions (Fig. S1) were also calculated (Fig. 1c). The global emissions of
 265 BaP were 7,166.9 t in 2013 and 7,109.5 t in 2018, respectively. **Figure. S3 shows emissions and changes**
 266 **for different sectors in China, Africa, South Asia, Europe, North America, and South America in**
 267 **2013 and 2018, where resident, industry, and agriculture are the main sources of BaP.** China is one
 268 of the largest BaP-emitting countries in the world. Its emissions were 1,952.2 t in 2013 and 1,750.2 t in
 269 2018, respectively, accounting for about 27.2% and 24.6% of the world, **which are generally consistent**
 270 **with the results of Shen et al. (2013) (20.3%). The residential sector is the largest emission source**
 271 **of BaP in China, accounting for 63.2% of the total emissions, followed by industrial sector (35.6%)**
 272 **in 2013. Africa and South Asia had the second and third-largest emissions, with residential**
 273 **combustion accounting for 87.3% and 84.0% of total emissions, respectively. This is related to the**
 274 **widespread use of biomass fuels for heating and cooking in developing countries (Shen et al., 2013).**

275 Emissions from China, Southern Africa, and South Asia accounted for 62.1% and 61.4% of the world.
276 China, Australia, South Asia, Europe, North America, South Korea, Japan, and North Korea displayed a
277 declining trend from 2013 to 2018. China experienced the largest decline (10.4%), due to the active
278 emission control measures taken under the “Air Pollution Prevention and Control Action Plan”
279 implemented in 2013. **The industrial sector contributed the most to the decline of BaP emissions,**
280 **followed by the residential combustion, which decreased by 18.9% and 5.1% from 2013 to 2018,**
281 **respectively, which are mainly related to the strengthened industrial emission standards, upgraded**
282 **industrial boilers, and the development of clean fuels. The above results are generally consistent**
283 **with the conclusions of Wang et al. (2021) in which PAHs emissions decreased by 11.36% from**
284 **2013 to 2017, with the industrial and residential sectors decreasing by 17.32% and 10.58%,**
285 **respectively. The emissions increased in Africa (10.3%) and South America (5.9%), mainly caused**
286 **by the emission increase in residential (10.6%) and agricultural (9.5%) sectors, respectively.**

287 To understand the change in BaP concentrations, we conducted five experiments: the first and
288 second experiments simulated the BaP concentration using the emissions in 2013 and 2018 driven by the
289 corresponding meteorological fields. The third experiment used the emission in 2018 but kept the
290 meteorological conditions in 2013 to investigate the effects of meteorological condition changes on the
291 concentration of BaP. Studies neglecting the heterogeneous loss of BaP and using two different
292 heterogeneous schemes were also performed to explore the impacts of heterogeneous reactions on BaP
293 concentrations in the fourth and fifth experiments

294 **3.2 Observational data**

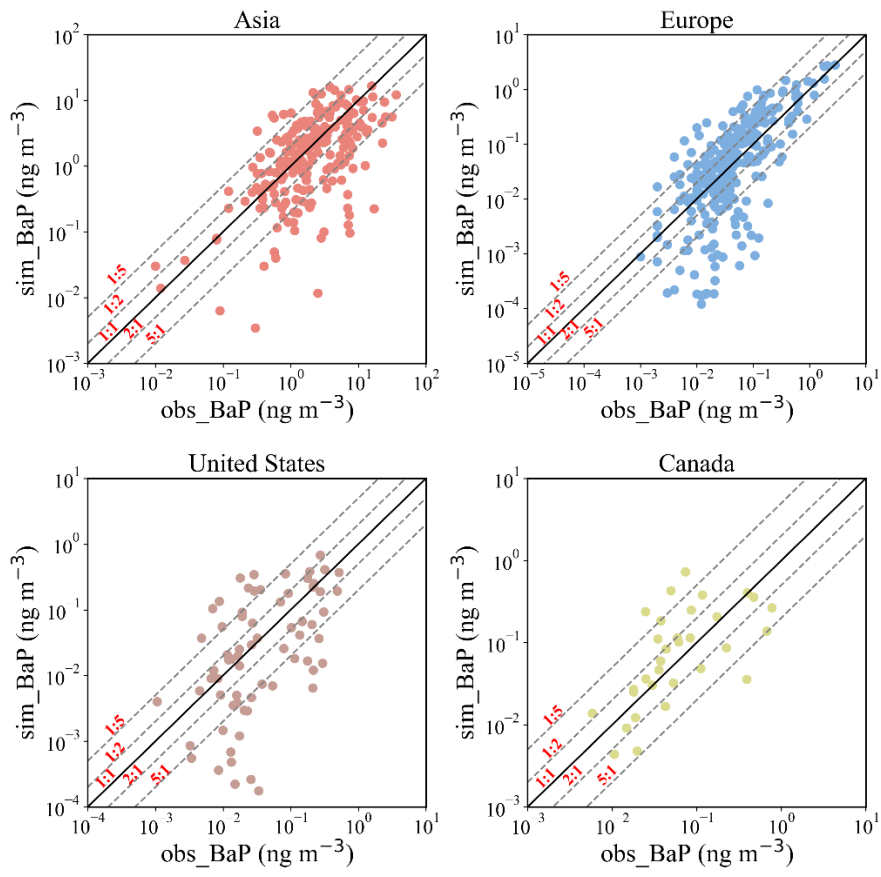
295 To evaluate the model performance, we collected the PAHs observation from several available
296 datasets and more than 50 published papers. The observational data are summarized as follows: (1)
297 European Monitoring and Evaluation Program (EMEP, available from
298 <https://projects.nilu.no/ccc/reports.html>, last access: 15 December 2023): this includes annual and
299 monthly averages of BaP concentrations at 36 European sites in Spain, Finland, France, Germany,
300 Norway, Poland, and other countries in Europe; (2) National Air Pollution Surveillance network: (NAPS,
301 <https://data-donnees.az.ec.gc.ca/data/air/monitor/>: last access: 30 January 2024): this includes daily
302 averages (autumn and winter) of BaP concentrations at Canadian stations; (3) Integrated Atmospheric
303 Deposition Network: (IADN, <https://iadnviz.iu.edu/datasets/index.html>, last access: 20 January 2023):

304 this includes monthly mean concentrations of BaP at 6 sites in the United States and Canada from 1990
305 to 2021; (4) Chinese Persistent Organic Pollutants (POPs) Soil and Air Monitoring Program Phase II
306 (SAMP-II, Ma et al., 2018): this is carried out by the International Joint Research Center for Persistent
307 Toxic Substances (IJRC-PTS), focusing on 11 urban centers in China (Beijing, Xi'an, Nanchang,
308 Kunming, Lanzhou, Chengdu, Harbin, Dalian, Lhasa, Guangzhou, and Shihezi), 1 suburb and 3
309 background/rural areas. This observational data only covers the period from August 2008 to July 2010;
310 (5) observational data collected from published papers (these sources are listed in supplementary material)
311 (Wu et al., 2024).

312 PAHs measurements data are very sparse compared to conventional pollutants (e.g., PM_{2.5}). Since
313 most of the data are not continuous in time, we selected data covering at least 10 days in years as close
314 as possible to the simulation year (2013) and used the mean values for comparison. The comparison of
315 the monthly variation was conducted only for sites in Europe where observations were continuous and
316 available. The locations of the BaP observation sites are shown in Fig. S2. The site information is listed
317 in Table S5 and Table S6.

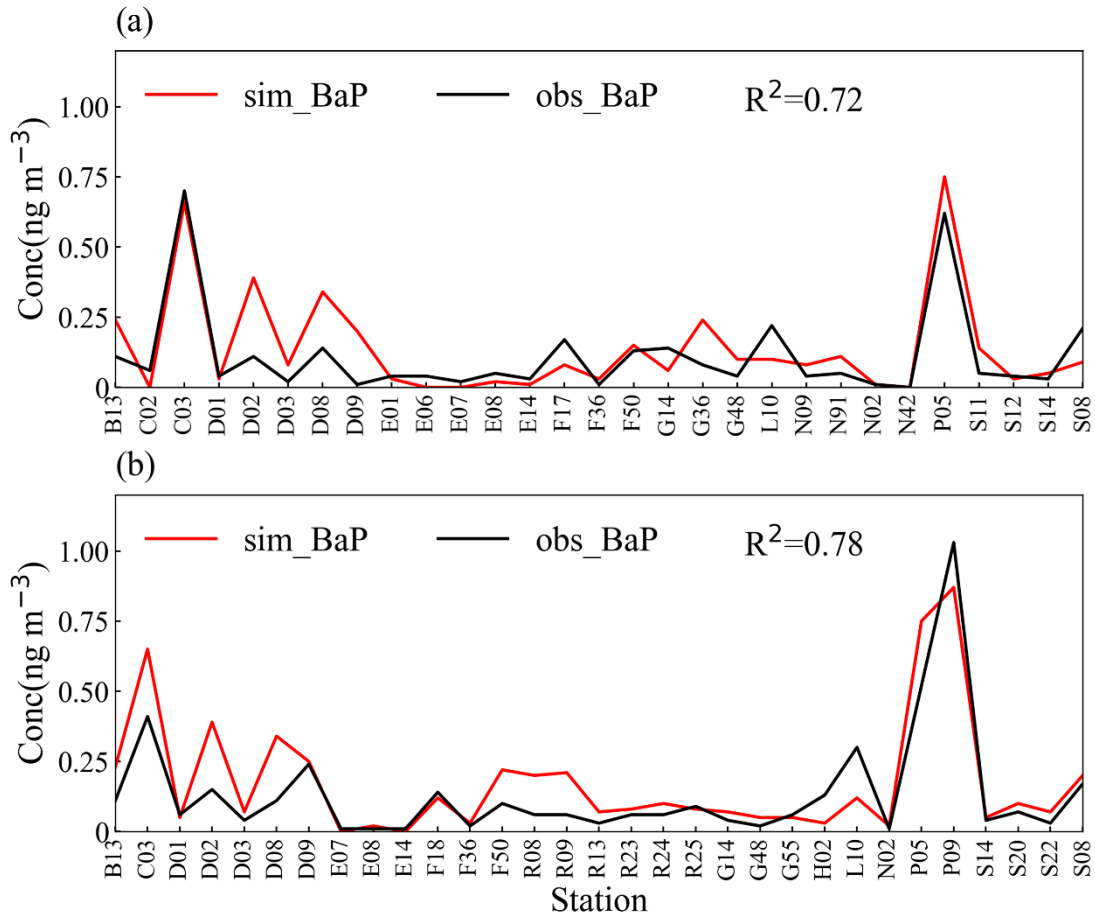
318 **4 Results**

319 **4.1 Global distribution of BaP and health risks**



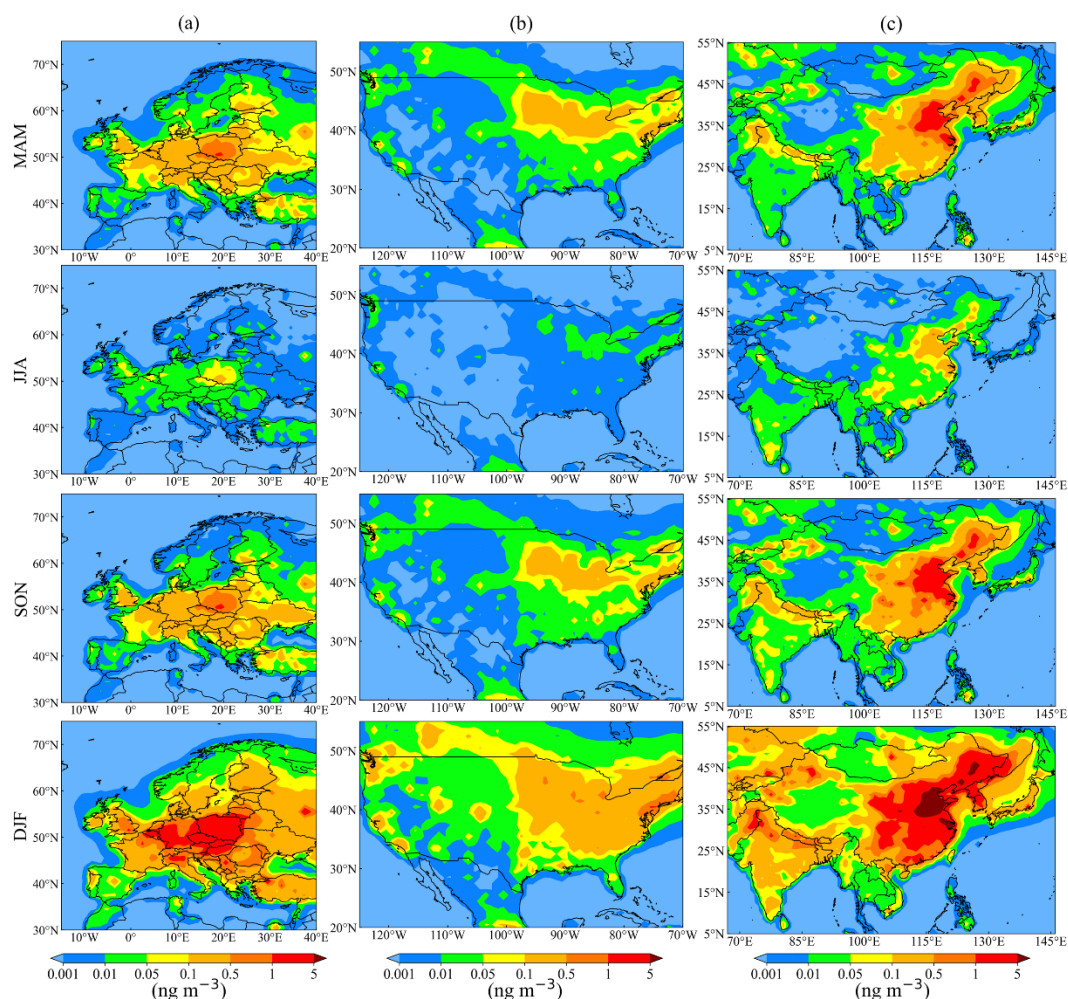
320
 321
 322
 323

Figure 2. Comparison of simulated (sim_BaP) and observed (obs_BaP) annual mean concentrations of BaP in Asia (pink), Europe (blue), United States (brown), and Canada (green) in 2013. The solid black line shows a ratio of 1 : 1 and the dashed gray lines show ratios of 5 : 1, 2 : 1, 1 : 2, and 1 : 5.



324
 325 **Figure 3. Comparison of the BaP annual mean simulated (red) concentrations with observed (black) values**
 326 **at European sites in (a) 2013 and (b) 2018.**

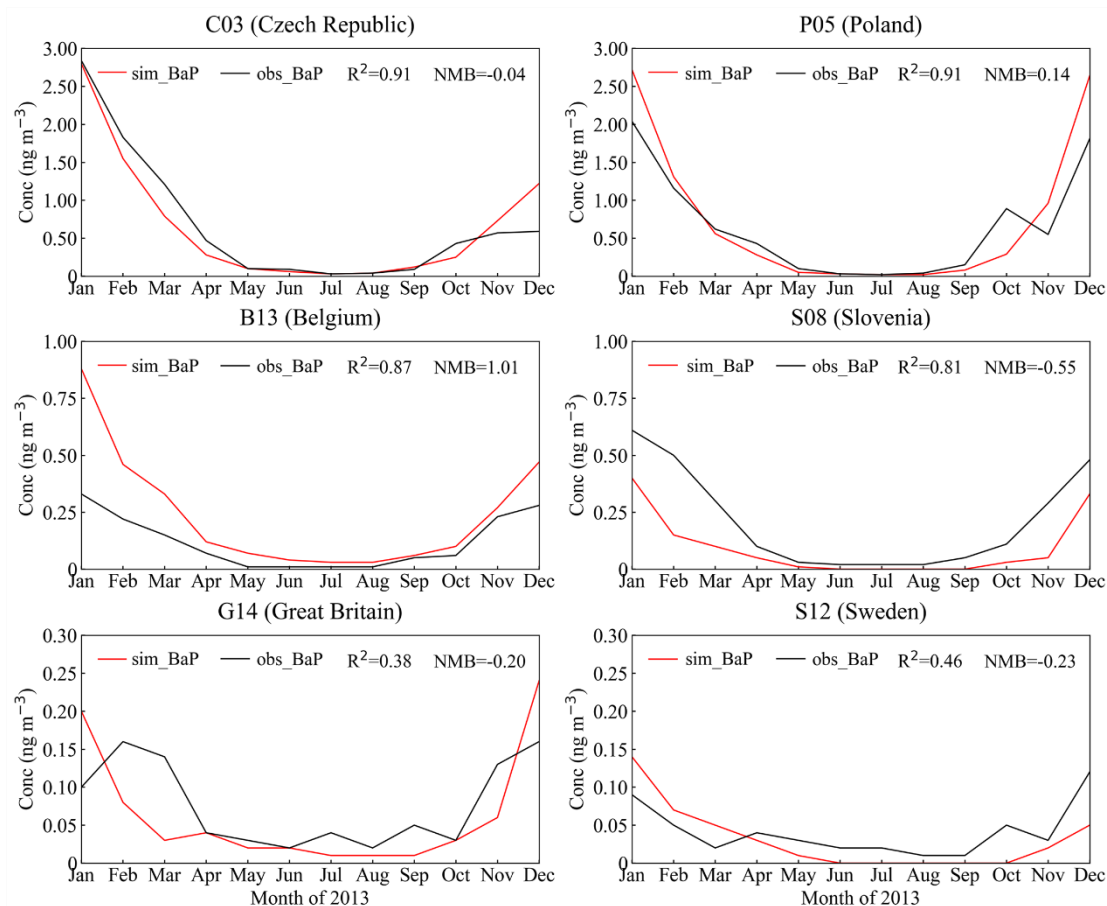
327 To evaluate the performance of the IAP-AACM model, annual mean simulated concentrations in
 328 Asia, Europe, the United States, and Canada were compared with observations (Fig. 2). The results show
 329 that the model can reproduce nearly half of the observation samples within a factor of 2 and most
 330 observations within a factor of 5 at sites in Asia, Europe, the United States, and Canada. The number of
 331 sites where BaP was underestimated was greater than the number where it was overestimated due to the
 332 averaging effect of subgrid emissions. Considering that some of the comparisons are not in the same year,
 333 a certain discrepancy between the model and observation is expected. Further, a specific comparison was
 334 performed using the data from about 30 stations in Europe (Fig. 3a and b). High concentrations were
 335 mainly found in polluted areas of Central Europe, consistent with the simulation of Gusev et al. (2017),
 336 such as Poland (P05) and the Czech Republic (C03) with observed values of 0.70 and 0.62 ng m⁻³,
 337 respectively, and simulated concentrations of 0.66 and 0.75 ng m⁻³ in 2013, The model successfully
 338 reproduced the observed concentrations and differences between sites.



339 **Figure 4. Spatial distributions of seasonal mean concentrations in (a) Europe, (b) the contiguous United**
 340 **States, and (c) East Asia in 2013.**
 341

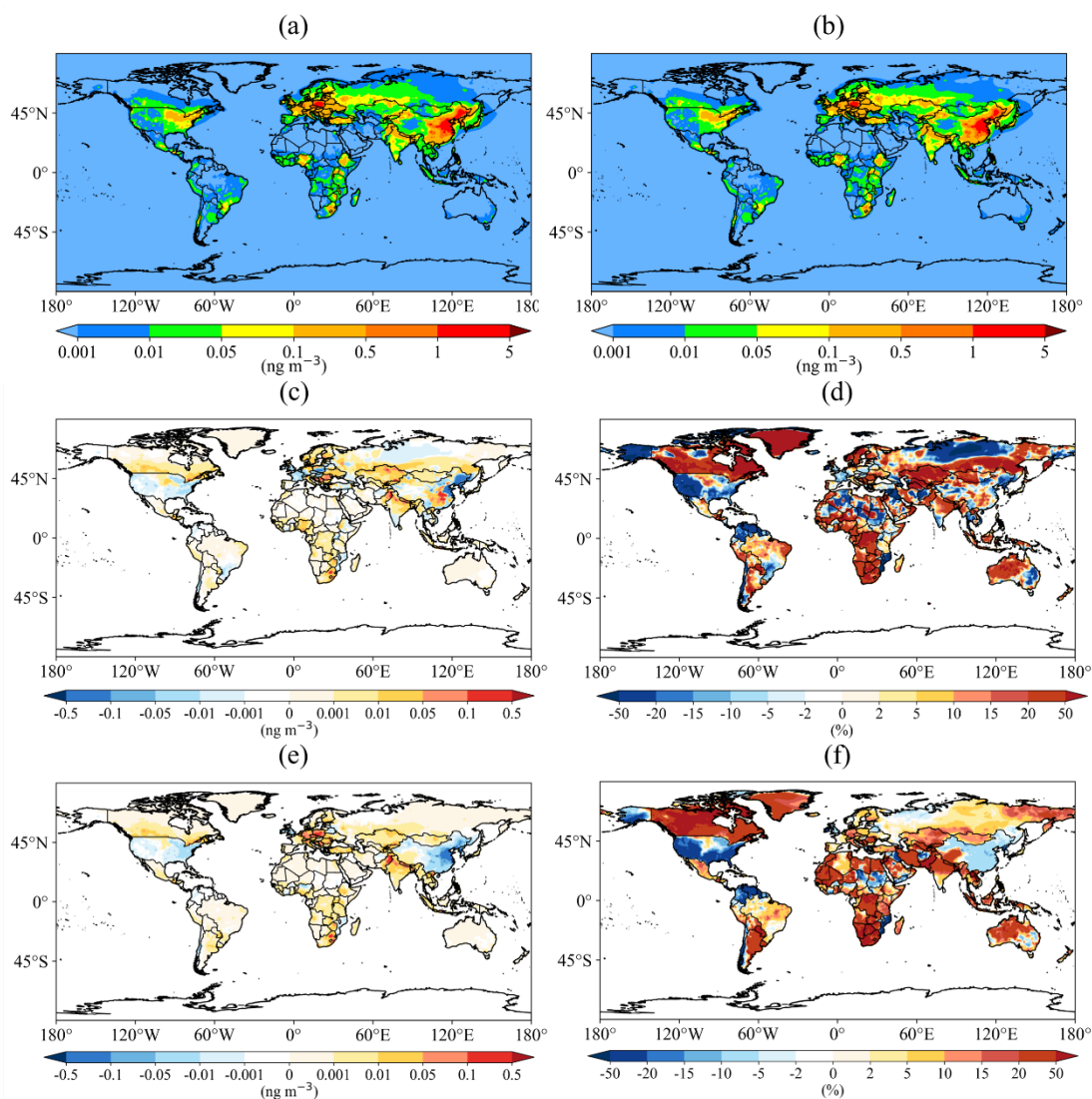
342 Figure 4 shows the seasonal mean concentrations of BaP in Europe, the contiguous United States,
 343 and East Asia in four seasons: March–April–May (MAM, representing spring), June–July–August (JJA,
 344 representing summer), September–October–November (SON, representing autumn), and December–
 345 January–February (DJF, representing winter). Generally, BaP had the highest concentration in winter and
 346 lowest in summer. This is caused by the larger emission and poorer atmospheric diffusion conditions in
 347 winter than in summer. In the contiguous United States, the concentrations were lower than 1 ng m^{-3}
 348 all four seasons, consistent with the simulation of Galarneau et al. (2014). In east China, large areas have
 349 a concentration of $> 1 \text{ ng m}^{-3}$ and even $> 5 \text{ ng m}^{-3}$ in BTH in winter. Europe shows a distribution of high
 350 values in central areas and low values in remote areas. In Central Europe (such as Poland and the Czech
 351 Republic), large areas have concentrations between $1\text{--}5 \text{ ng m}^{-3}$ in winter. High concentrations were also
 352 reported by Bieser et al. (2012). The observation clearly shows higher concentrations at sites in Poland
 353 and the Czech Republic than at other sites in Europe (Fig. 5). The model successfully reproduces the

354 seasonal variation of BaP at sites in Europe. The simulation had a good agreement with observations at
 355 C03 and P05 with correlation coefficient (R^2) of 0.91 and 0.91, and normalized mean bias (NMB) of -
 356 0.04 and 0.14, respectively. The R^2 was higher than 0.8 at B13 and S08, and the NMB was 1.01 and -
 357 0.55. In summary, IAP-AACM can reasonably simulate the spatial distribution and seasonal variation of
 358 BaP.



359
 360
 361

Figure 5. Comparison of the BaP month mean simulated concentrations (red) with observed values (black) at six stations in Europe in 2013.

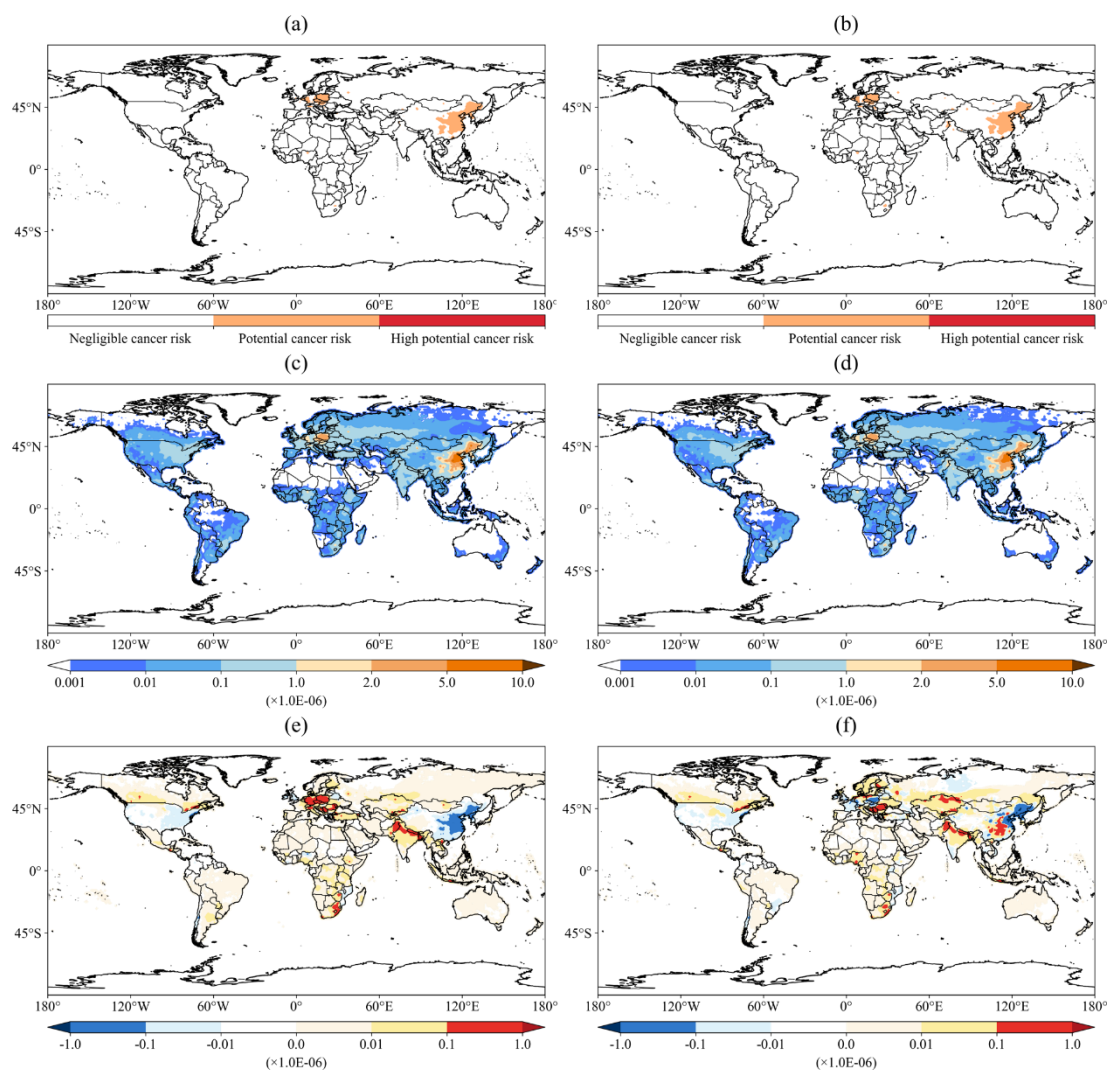


362

363 **Figure 6. Spatial distributions of annual mean BaP concentrations based on the EDGAR in (a) 2013 and (b)**
 364 **2018 . The (c/e) absolute and (d/f) relative concentration changes from 2013 to 2018 are shown considering**
 365 **(c, d) both emissions and meteorological conditions or (e, f) only emissions, respectively.**

366 The spatial distribution of annual mean BaP concentrations based on the EDGAR inventory in 2013
 367 and 2018 are shown in Fig. 6a and b. The spatial distribution of BaP concentrations in 2018 was similar
 368 to that in 2013. The spatial pattern was consistent with the emission distribution in the EDGAR inventory.
 369 High concentrations of BaP were found in northern and eastern China, and central Europe, even
 370 exceeding the European Union target value for BaP (1 ng m⁻³), indicating an urgent need to control BaP
 371 and other PAHs. The absolute and relative concentration changes from 2013 to 2018 are shown in Fig.
 372 6c and d. The most significant decreases were seen in Russia, the United States, eastern and northern
 373 China. By contrast, the concentration in India, Europe, Southeast Asia, and South Africa shows an
 374 increase, with the average annual concentration increasing by 19.4%, 1.2%, 11.2%, and 18.3%,

375 respectively. When only considering the impact of emission change (Fig. 6e and f), the decrease in the
 376 eastern United States is larger and the increase in central Europe is larger. In particular, there is an obvious
 377 decline (about 8.0%) across China, which demonstrates the effect of the emission reduction measures.
 378 These results clearly show the large influence of meteorological changes. It is crucial to consider
 379 meteorological factors when evaluating emission changes and reduction measures through monitoring
 380 concentrations in the atmosphere.



381 **Figure 7. The distribution of health risks grade in (a) 2013 and (b) 2018, the distribution of TILCR in (c)**
 382 **2013 and (d) 2018, and the absolute from 2013 to 2018 when considering the change in (e) emissions only, (f)**
 383 **both emissions and meteorological conditions.**

385 **The global distribution of health risks grade and TILCR (the sum of ILCR values of the two**
 386 **exposure routes after averaging the parameters of the different groups) in 2013 and 2018 are shown**
 387 **in Fig. 7. It can be seen that most of the countries just face negligible cancer risk, and no regions**
 388 **facing high potential cancer risk when evaluation is based on annual mean concentration. However,**

389 eastern China and central Europe are in potential cancer risk, with the highest TILCR values of
390 1.54×10^{-5} (1.47×10^{-5}) and 4.62×10^{-6} (4.23×10^{-6}) in 2013 (2018), respectively. It should be noted that
391 in other developing countries such as Africa, India, and Southeast Asia, TILCR values increased
392 in 2018 compared to 2013, with the highest (mean) values increasing from 1.47×10^{-6} (4.15×10^{-8}) to
393 2.26×10^{-6} (4.78×10^{-8}), from 1.41×10^{-6} (2.03×10^{-7}) to 1.73×10^{-6} (2.43×10^{-7}), and from 8.02×10^{-7} (6.07
394 $\times 10^{-8}$) to 1.14×10^{-6} (6.75×10^{-8}), respectively. These countries will be likely to face potential even high
395 potential cancer risks, especially in winter. In addition, Lou et al. (2023) has indicated that health
396 risks in South Asia and Africa will increase in the future with the increase of residential fuels use
397 along with the population growth in these regions. It is clear that clean development is a necessary
398 consideration for developing countries to avoid the health risks posed by PAHs.

399 4.2 Distribution of PAHs and their change in China

400 Figure 8 shows the annual mean distribution of BaP in China in 2013. The concentrations ranged
401 from 0.02 to 6.14 ng m⁻³. Overall, high concentrations were simulated in the North China Plain, East
402 China, and Northeast China, significantly higher than in Northwest and Southwest China, consistent with
403 previous studies (Ma et al., 2020; Yan et al., 2019). This can be largely attributed to the industrial
404 and residential coal combustion in these regions. Among the different provinces in China, there are
405 14 provinces with concentrations higher than the ambient air quality standards of China (1 ng m⁻³, GB
406 3095–2012: <http://www.zhb.gov.cn/>, last access: 6 April 2014). Shanghai had the highest concentration
407 of 6.14 ng m⁻³, followed by Tianjin (4.56 ng m⁻³), Beijing (3.41 ng m⁻³), and Shandong (3.10 ng m⁻³).
408 The concentrations in the Northwest and Southwest regions were lower, with Tibet having the lowest
409 concentration of only 0.02 ng m⁻³. This is due to lower levels of industrial activities and population
410 density in these regions compared to eastern regions. In addition, the high topography of northwest
411 regions has good air circulation and is conducive to the diffusion and dilution of atmospheric pollutants.
412 In 2013, Beijing had the highest BaP concentration in winter (14.03 ng m⁻³), possibly due to the high
413 population density, high number of vehicles, and frequent industrial activities in Beijing. Moreover,
414 Beijing lies on the North China Plain, where the meteorological conditions make it easier for air
415 pollutants to stay and accumulate, resulting in a high concentration of BaP.

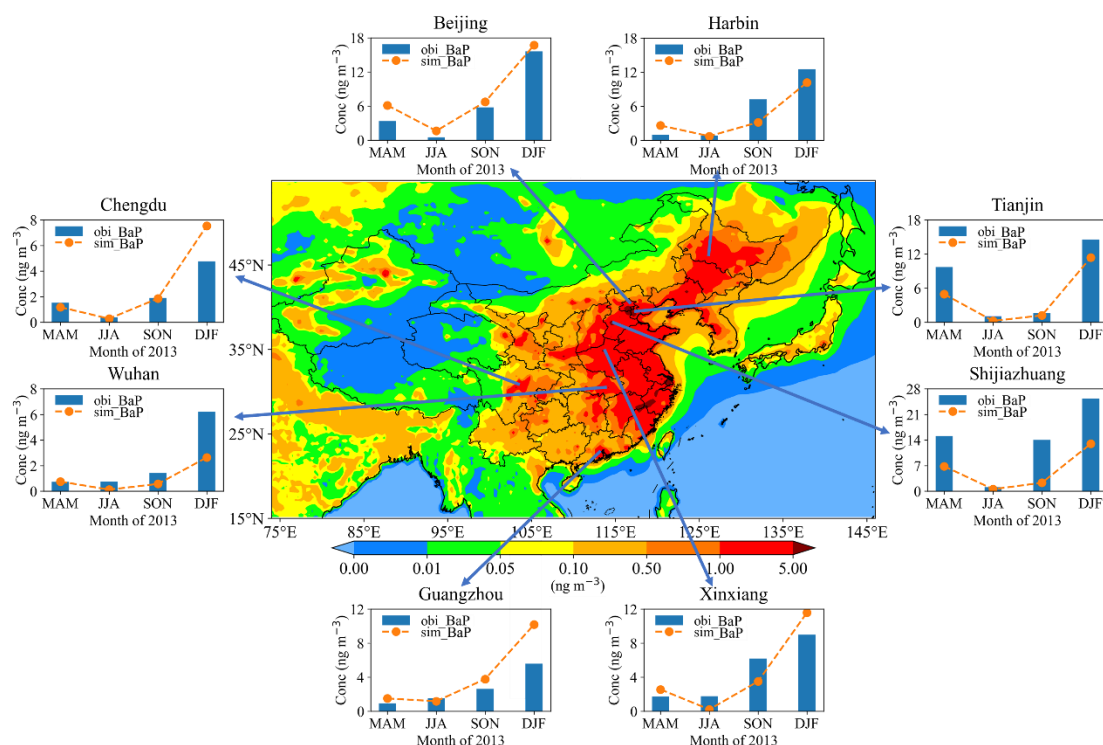


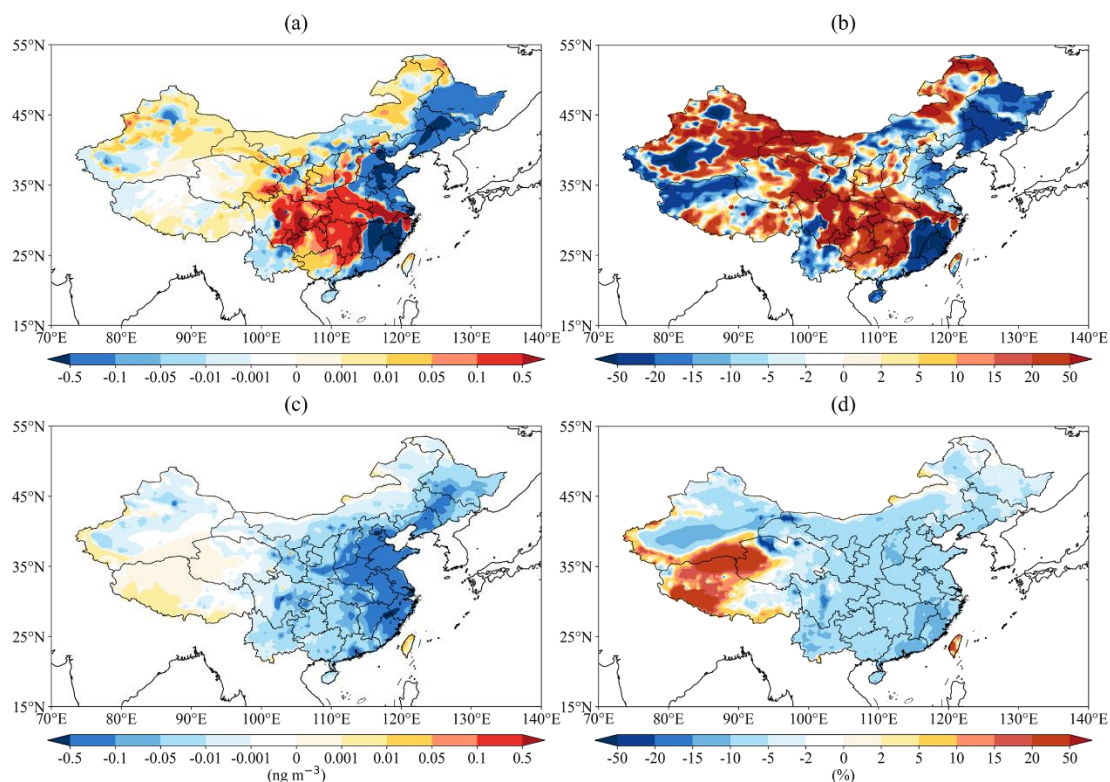
Figure 8. Spatial distributions of annual mean concentrations in China. Comparison of the BaP month mean simulated concentrations (orange) with observed values (blue) at eight cities in 2013.

416
417
418

419 To reveal the seasonal variation of BaP concentrations in key regions, we analyzed the concentration
420 in eight major cities, i.e., Beijing, Tianjin, Shijiazhuang, Xinxiang, Wuhan, Chengdu, Guangzhou, and
421 Harbin (seen in Fig. 8). It can be seen that the seasonal variations of BaP in these cities are similar, with
422 the highest values in winter and the lowest in summer. The seasonal difference in northern cities was
423 significantly greater than that in southern cities. In Beijing, Xinxiang, Tianjin, Harbin, and Shijiazhuang,
424 the differences in concentration between winter and summer were as high as 15.06, 11.76, 11.14, 9.45,
425 and 12.42 ng m^{-3} , respectively. This is caused by the fact that coal-fired heating is very common in
426 northern China, which can significantly increase the PAH emissions in winter (Yan et al., 2019). In
427 addition, the meteorological conditions also affect the seasonal variation of PAHs, as the lower
428 temperature, less rainfall, and weaker solar radiation during the winter support the formation of a stable
429 inversion layer, greatly limiting the diffusion of BaP in the air (Lin et al., 2015; Quan et al., 2014).

430 By comparing the simulated concentrations with the observed concentrations, we find that the model
431 can capture the BaP concentrations and the seasonal pattern in different cities. For example, the observed
432 and simulated concentrations show good consistency in the spring, summer, and autumn of Chengdu and
433 in the summer, autumn, and winter of Beijing, with a deviation of only 0.04 to 1.1 ng m^{-3} . However, there
434 were some deviations between the simulated and observed concentrations. The most obvious

435 underestimation is seen in Shijiazhuang. This is probably due to the underestimation of emissions and
 436 the model resolution that may not fully resolve the pollution in cities with urban areas smaller than the
 437 model grid. The model performance could be improved by using more precise emissions and increasing
 438 grid resolution. Nonetheless, the model can capture the magnitude and seasonal variation in BaP
 439 concentration well in China and in other countries around the world, and can therefore be used to evaluate
 440 the health effects of BaP exposure.

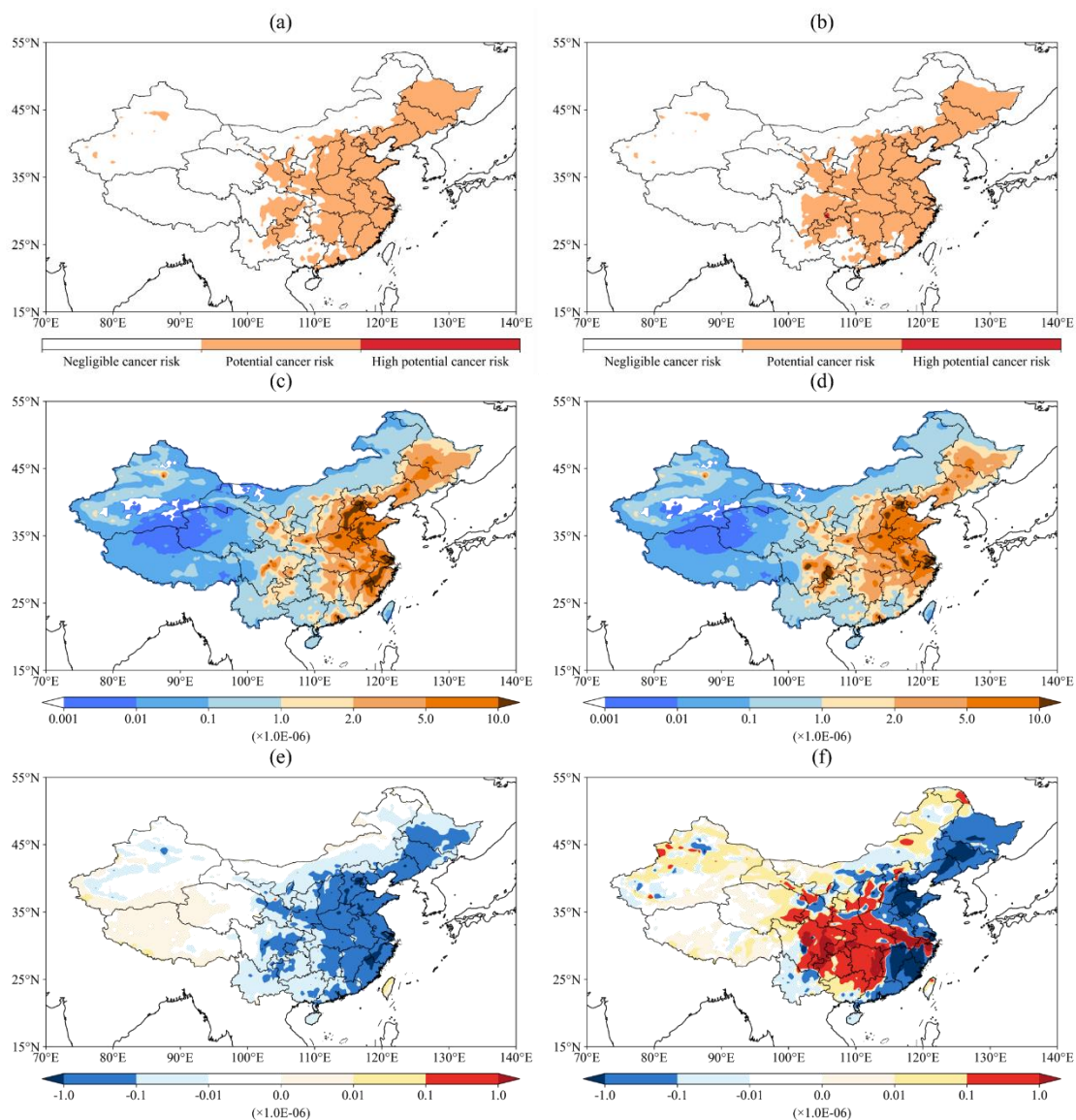


441 **Figure 9. The (a/c) absolute and (b/d) relative concentration changes from 2013 to 2018 in mean annual BaP**
 442 **concentrations in China are shown considering (a, b) both emissions and meteorological conditions or (c, d)**
 443 **only emissions, respectively.**

445 The changes from 2013 to 2018 are shown in Fig. 9. The trend and magnitude of changes differ
 446 greatly across different regions. The largest decrease ($> 20\%$) was seen in northeastern and southeastern
 447 China, **consistent with the other studies in Beijing (Lin et al., 2024), Shanghai (Yang et al., 2021),**
 448 **Shenyang (Zhang et al., 2023), Tianjin (Zhang et al., 2022).** The concentration also decreased in the
 449 North China Plain, **benefitting from the emission reduction policies such as the development of**
 450 **cleaner energy sources and the control of industrial emissions.** The concentration decrease was larger
 451 than the emission reduction over these areas. By contrast, as shown in Fig. 9a, the concentration in the
 452 Sichuan Basin showed an inverse trend although the emission decreased. **This phenomenon**

453 demonstrates the large impact of unfavorable meteorological conditions with decreasing
454 temperatures and planetary boundary layer height compared to 2013 (Ding et al., 2019). When only
455 considering the emissions changes, the concentration shows a decrease over most regions consistent with
456 the emission change. It should be noted that the decrease in BaP in the two experiments is significantly
457 lower than that of PM_{2.5}. As shown in Fig. 9b (Fig. 9d), the BaP concentration decreased by 9.1%
458 and 6.7% (8.5% and 9.4%) in the BTH and the YRD, respectively. Wang et al. (2019) showed that
459 compared with 2013, the concentration of PM_{2.5} in the BTH, the YRD, and the PRD in 2017 decreased
460 by 39.6%, 34.3%, and 27.7%, respectively. For cities in North and East China, the concentration still
461 exceeds the national limit value (1 ng m⁻³) although the concentration of BaP decreased significantly in
462 2018. For example, the BaP concentrations in Shanghai, Beijing, and Tianjin considering changes in both
463 emissions and meteorology were 5.32, 3.31, and 3.38 ng m⁻³, respectively, and those with emission
464 changes alone were 5.58, 3.11, and 4.17 ng m⁻³, indicating that the concentrations are mainly affected by
465 the emission sources. The results in the central and western cities differed greatly between the two
466 experiments, especially in Chongqing, Sichuan, and Guizhou, indicating that changes were mainly
467 related to meteorological conditions. Therefore, when formulating emission reduction policies, it is
468 necessary to take into account the effects of changes in meteorological conditions as well as emission
469 sources.

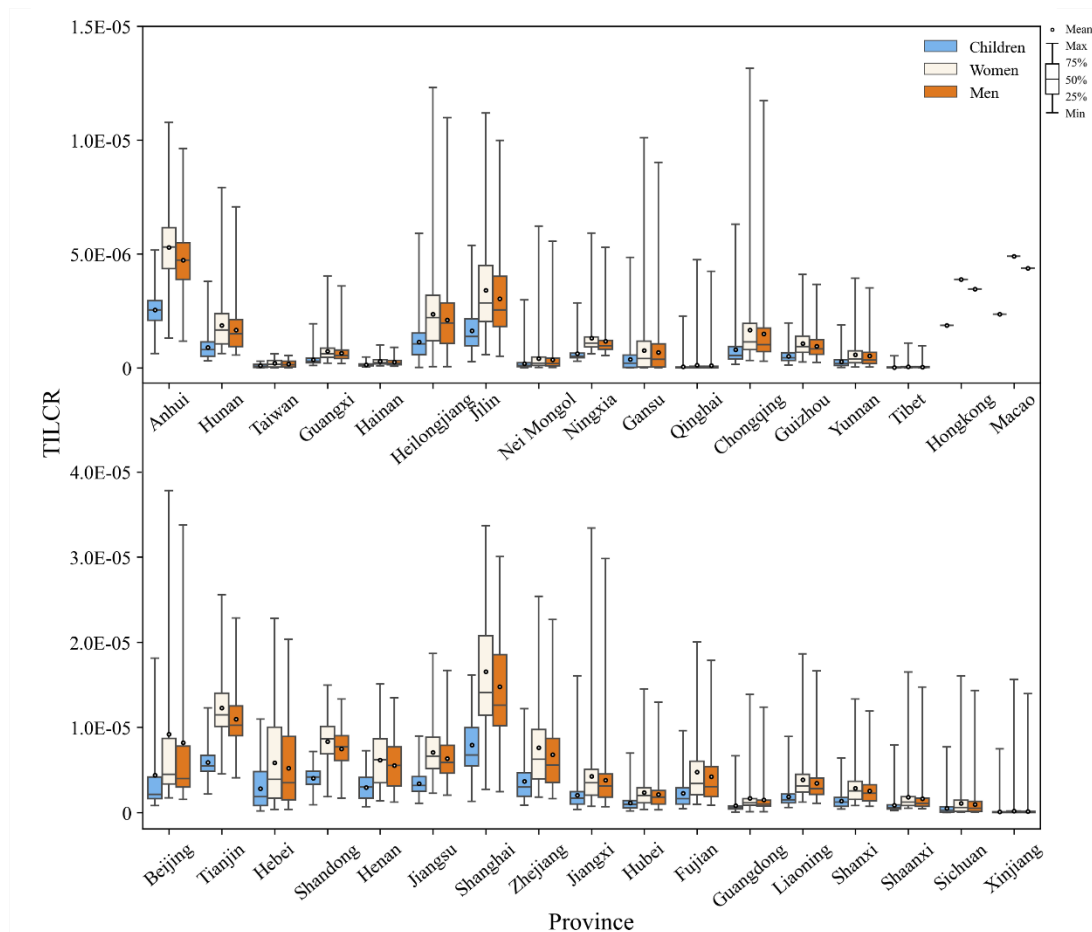
470 4.3 Health risks of PAHs in China



471
 472 **Figure 10. The distribution of health risks grade in China in (a) 2013 and (b) 2018, the distribution of**
 473 **TILCR in (c) 2013 and (d) 2018, and the TILCR changes from 2013 to 2018 when considering the change in**
 474 **(e) emissions only, (f) both emissions and meteorological conditions.**

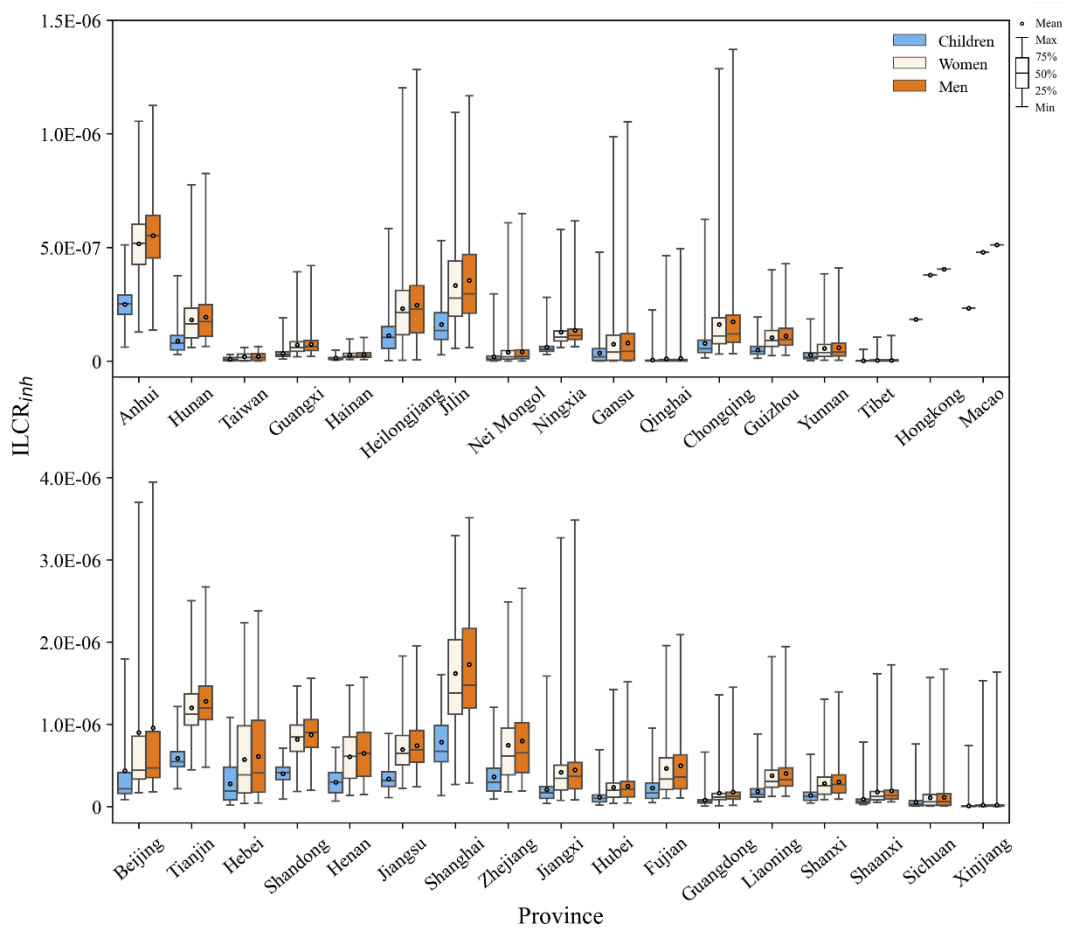
475 In this section, the health risks of BaP are assessed based on the simulation over the nested domain
 476 (domain 2) covering China. **As shown in Fig. 10a and b, the health risks in western China is negligible,**
 477 **while there is a potential cancer risk in eastern China. Figure 9c and d show the TILCR values in**
 478 **2013 and 2018,** and Fig. 10e and f show the change from 2013 to 2018 when only emissions or both
 479 emissions and meteorological conditions are considered. It can be seen that the spatial distribution of
 480 TILCR (Fig. 10c) is consistent with the spatial distribution of the BaP annual concentrations (Fig. 6),
 481 showing higher risk in eastern regions than in the western regions (Han et al., 2020). The values of the
 482 TILCR in China ranged from 3.0×10^{-9} to 3.5×10^{-5} , with an average value of 1.4×10^{-6} . Compared with

483 2013, the average TILCR in 2018 decreased by 8.0×10^{-8} , which is mainly directly related to the decrease
 484 in concentration. From the perspective of two exposure routes, $ILCR_{inh}$ and $ILCR_{der}$ values ranged from
 485 2.8×10^{-10} – 3.3×10^{-6} and 2.7×10^{-9} – 3.2×10^{-5} , with an average value of 1.3×10^{-2} and 1.3×10^{-6} , respectively.
 486 The values of $ILCR_{der}$ were one order of magnitude higher than the $ILCR_{inh}$.



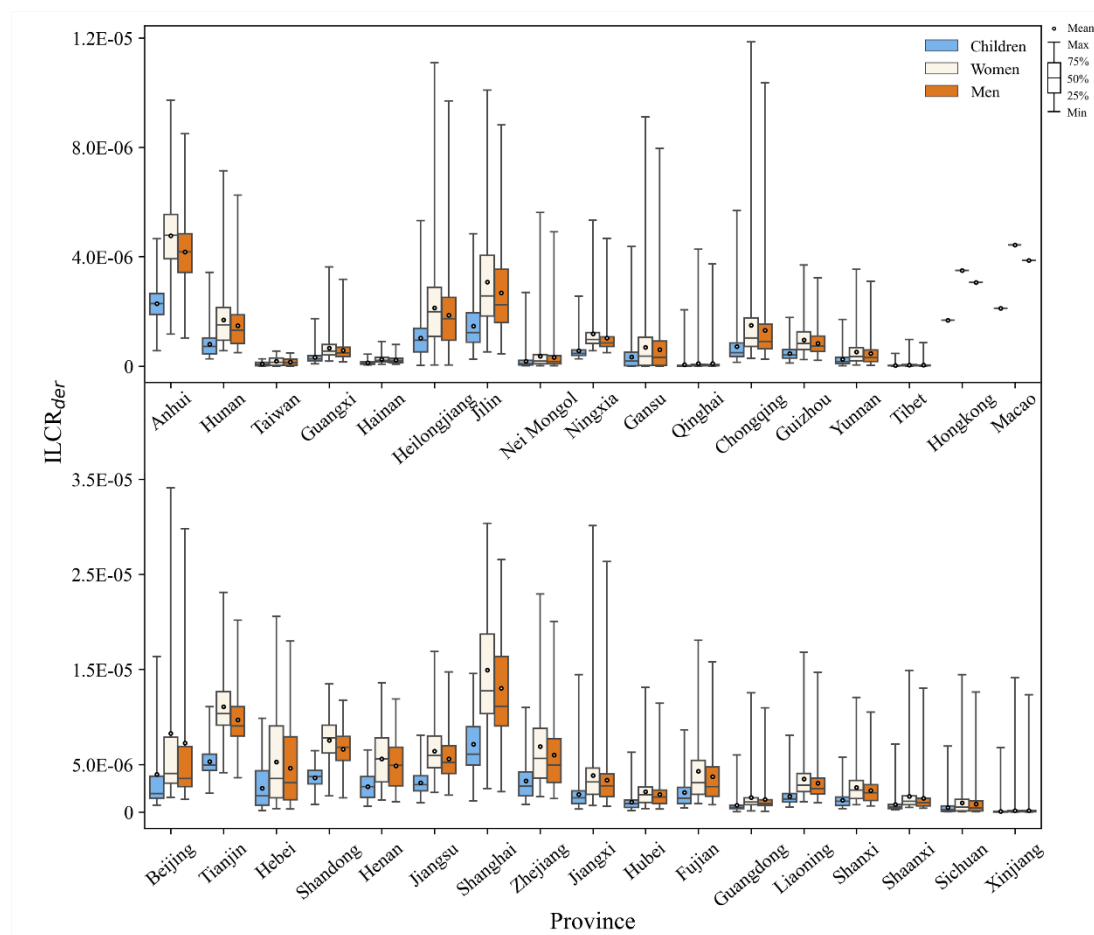
487
 488 **Figure 11. The TILCR values for the three age groups (Children, Women, and Men) in different provinces**
 489 **of China in 2013.**

490 The TILCR values of the three groups in 2013 and 2018 **calculated using Eq. (14)-Eq. (18)** are
 491 shown in Fig. 11 and Fig. S4, respectively, which ranged from 1.55×10^{-9} to 3.78×10^{-5} (1.60×10^{-9} to
 492 3.41×10^{-5}). The order of TILCR was women (1.46×10^{-6}) > men (1.31×10^{-6}) > children (7.03×10^{-7}), which
 493 was similar to that of dermal contact exposure. Overall, 29.2% of TILCR were higher than 1.0×10^{-6} , and
 494 1.2% of TILCR were higher than 1.0×10^{-5} in 2013. There was a slight decrease in TILCR values in 2018
 495 due to the lower concentrations of BaP, with 27.9% and 0.7% of TILCR higher than 1.0×10^{-6} and 1.0×10^{-5} ,
 496 respectively. There is no high cancer risk in China, but there are potential cancer risks in some areas,
 497 which should be paid attention to.



498
 499
 500

Figure 12. The ILCR_{inh} values for the three age groups (Children, Women, and Men) in different provinces of China in 2013.



501
502
503

Figure 13. The ILCR_{der} values for the three age groups (Children, Women, and Men) in different provinces of China in 2013.

504 The ILCR values of the three groups in China through inhalation and dermal exposure routes are
 505 shown in Fig. 12 and Fig. 13, and the ILCR in 2018 are shown in Fig. S5 and Fig. S6. For the inhalation
 506 pathway, the average ILCR_{inh} was 1.22×10^{-7} ($< 1.0 \times 10^{-6}$). The order of ILCR_{inh} was men (1.53×10^{-7}) >
 507 women (1.43×10^{-7}) > children (6.95×10^{-8}), and the risk for men was about twice that of children, but was
 508 lower in women than in men. This may be caused by the fact that the inhalation and metabolic rate of
 509 women are weaker than men (Bai et al., 2020). The highest average value was found in Shanghai, where
 510 the average ILCR_{ing} for the three groups were 1.72×10^{-6} , 1.62×10^{-6} , and 7.84×10^{-7} , respectively. Han et
 511 al. (2020) found cases of excess cancer due to exposure to PAHs in large cities such as Shanghai. Only
 512 1.6% of the three groups had ILCR_{ing} higher than 1×10^{-6} , indicating that the health risks from inhalation
 513 exposure were low. A similar conclusion was mentioned in an earlier review (Yan et al., 2019).

514 For dermal contact exposure, the average ILCR_{der} was 1.04×10^{-6} ($> 1.0 \times 10^{-6}$). Compared to the
 515 ILCR_{inh}, the health risk to adults was slightly higher than that to children, but women had higher risk

516 values than men. This may be caused by the fact that the body weight of women is weaker than men. The
517 order of $ILCR_{der}$ was women (1.32×10^{-6}) > men (1.15×10^{-6}) > children (6.33×10^{-6}), which is similar to
518 the results of previous studies (Bai et al., 2020). Among the three groups, 27.4% of the $ILCR_{der}$ values
519 were higher than 1×10^{-6} , and 0.7% were higher than 1×10^{-5} . This shows that there is a greater potential
520 carcinogenic risk through dermal contact exposure.

521 **5 Discussion**

522 It should be noted that model results have some uncertainties even though our model simulated the
523 main features of PAHs concentrations reasonably well. Firstly, we simulated lower BaP concentrations
524 when using the PKU inventory than when using the EDGAR inventory over most continental areas,
525 except for Inner Mongolia, eastern Russia, and north China (Fig. S7). The difference can be as high as
526 0.5 ng m^{-3} over some areas in wintertime although the spatial and temporal distributions are consistent.
527 The emission inventory remains to be constrained by more observations. Current observations are too
528 sparse to conduct detailed evaluation in areas where long-term measurements are not available. Secondly,
529 we tested the influence of heterogeneous reaction schemes on simulation. When heterogeneous reactions
530 were not considered, the model significantly overestimated the concentration of BaP (Fig. S8), suggesting
531 the importance of heterogeneous loss of BaP. Using the Langmuir-Hinshelwood mechanism, we
532 simulated lower concentrations in most regions of the northern hemisphere, especially in winter (Fig.
533 S9). However, the difference between the simulated results of the two mechanisms is significantly
534 reduced in summer due to high temperature and high humidity. This is consistent with the results by Mu
535 et al. (2018), i.e., low temperature and low humidity can significantly increase the lifetime of BaP.
536 Comparison of model results using different schemes and model intercomparison would further help
537 identify the uncertainties and improve model performance.

538 **6 Conclusion**

539 In this study, the PAHs modules were coupled into the IAP-AACM model to investigate the global
540 and regional distribution of PAHs. The model has the state-of-the-art heterogeneous mechanism and
541 allows us to consistently examine the multi-scale distribution of PAHs. Comparison with observations
542 shows that the model can reproduce the different concentrations of BaP at the stations in Asia, Europe,

543 the United States, and Canada. The model can capture the seasonal variation of BaP, with lower
544 concentrations in summer and higher concentrations in winter over the continents in the northern
545 hemisphere. The global distributions of BaP in 2013 and 2018 were very similar, with high concentrations
546 concentrated in eastern China and central Europe, even exceeding EU limits (1 ng m^{-3}). Compared with
547 2013, BaP concentration in 2018 showed a decrease in the United States, Poland, France, Czech, and
548 some regions in China. By contrast, the concentrations increased by $>10\%$ in India and South Africa.
549 Populations in these regions are facing increased health risks posed by PAHs.

550 In China, the decline in BTH (8.5%) and YRD (9.4%) benefitted from “the Action Plan”. However,
551 the decline was significantly less than that of conventional pollutants, such as $\text{PM}_{2.5}$. Changes in
552 meteorological conditions had a significant influence on changes in BaP concentration, which increased
553 in the Sichuan Basin and central China even though the emissions over these areas decreased due to the
554 control measures. There was a slight decrease in total ILCR (TILCR) values in 2018 compared to 2013.
555 For the different exposure routes, the dermal contact was an order of magnitude higher than the inhalation
556 route. The TILCR for adults was greater than that for children. 29.2% of TILCR were higher than 1.0×10^{-6} ,
557 indicating that there are still potential cancer risks in China. More attention must be paid to the non-
558 traditional pollutant pollutants and strict but different control measures are necessary to reduce PAHs'
559 concentration and health risks. **Especially in the fall and winter seasons, the concentration of BaP
560 and the associated health risk is significantly higher than in other seasons. Management efforts on
561 key sectors (e.g., industrial and residential sources) should be further strengthened. In heavily
562 polluted cities, using clean energy to replace coal combustion, adjusting the energy structure of
563 factory production, and developing innovative technologies with lower and even no emissions
564 would be helpful to reduce PAHs pollution.**

565 In summary, our study developed an effective tool for simulating the global and regional
566 concentrations of BaP and other PAHs and quantified the health risks in China from 2013 to 2018. Model
567 analysis indicated that emission inventories and heterogeneous reactions can significantly affect the
568 simulated BaP concentrations. Accurate emissions and reasonable representation of heterogeneous
569 reactions would greatly reduce the gap between model results and observation. However, the current
570 observations are insufficient to fully evaluate and constrain the model. Especially, long-term observations
571 are needed in Asia, India, and Africa. These regions are still facing significant health risks. In addition,

572 monitoring in the background and remote regions (such as the Arctic) is necessary to quantify the long-
573 range transport of PAHs.

574

575 *Code and data availability.* The source code and their introduction of IAP-AACM can be found online
576 via Zenodo (<https://doi.org/10.5281/zenodo.12214119>). The simulated data can be found via Zenodo
577 (<https://doi.org/10.5281/zenodo.11595165>). All the observational data are provided in the supplement
578 and can be found via Zenodo (<https://doi.org/10.5281/zenodo.11595165>).

579

580 *Author contributions.* ZcW developed the model, prepared the input data, performed the simulations and
581 analysis, and wrote the paper with suggestions from all co-authors. XC supported the coding and
582 conceived the idea of the paper. XC and ZfW revised the paper and provided scientific guidance through
583 all research advances. JL, ZW, LW, HC, YL, MQ, XT, and QW modified the manuscript. WW supported
584 the emission data. YW, ZZ, and ZJ supported the data analysis. All listed authors have read and approved
585 the final manuscript.

586

587 *Competing interests.* The authors declare that they have no conflict of interest.

588

589 *Disclaimer.* Publisher's note: Copernicus Publications remains neutral about jurisdictional claims in
590 published maps and institutional affiliations.

591

592 *Acknowledgements.* We are particularly grateful to Prof. Oliver Wild at Lancaster University for his help
593 with improving the paper. We thank Prof. Alexey Gusev at EMEP for providing MSC-E results as a good
594 reference to test our model performance. We also thank the National Key Scientific and Technological
595 Infrastructure project "Earth System Science Numerical Simulator Facility" (EarthLab).

596

597 *Financial support.* This research has been supported by the National Key R&D Program of China (Grant
598 NO.2020YFA0607801), the National Natural Science Foundation of China (Grant NO. 42377105) and
599 the National Key Scientific and Technological Infrastructure project "Earth System Science Numerical
600 Simulator Facility".

601 **References**

- 602 Aulinger, A., Matthias, V., Quante, M.: CMAQ simulations of the benzo(a)pyrene distribution over
603 Europe for 2000 and 2001, *Atmospheric Environment*, 43, 4078-4086,
604 <https://doi.org/10.1016/j.atmosenv.2009.04.058>, 2009.
- 605 Aulinger, A., Quante, M., Matthias, V.: Introducing a Partitioning Mechanism for PAHs into the
606 Community Multiscale Air Quality Modeling System and Its Application to Simulating the
607 Transport of Benzo(a)pyrene over Europe, *Journal of Applied Meteorology and Climatology*,
608 46, 1718-1730, <https://doi.org/10.1175/2007jamc1395.1>, 2007.
- 609 Baek, S. O., Field, R. A., Goldstone, M. E., Kirk, P. W., Lester, J. N., Perry, R.: A review of atmospheric
610 polycyclic aromatic-hydrocarbons-sources, fate and behavior, *Water Air and Soil Pollution*, 60,
611 279-300, <https://doi.org/10.1007/bf00282628>, 1991.
- 612 Bai, L., Chen, W. Y., He, Z. J., Sun, S. Y., Qin, J.: Pollution characteristics, sources and health risk
613 assessment of polycyclic aromatic hydrocarbons in PM_{2.5} in an office building in northern
614 areas, China, *Sustainable Cities and Society*, 53, 10, <https://doi.org/10.1016/j.scs.2019.101891>,
615 2020.
- 616 Bieser, J., Aulinger, A., Matthias, V., Quante, M.: Impact of Emission Reductions between 1980 and 2020
617 on Atmospheric Benzo (a) pyrene Concentrations over Europe, *Water Air and Soil Pollution*,
618 223, 1393-1414, <https://doi.org/10.1007/s11270-011-0953-z>, 2012.
- 619 Byun, D., Schere, K. L.: Review of the governing equations, computational algorithms, and other
620 components of the models-3 Community Multiscale Air Quality (CMAQ) modeling system,
621 *Applied Mechanics Reviews*, 59, 51-77, <https://doi.org/10.1115/1.2128636>, 2006.
- 622 Byun, D. W., Dennis, R.: DESIGN ARTIFACTS IN EULERIAN AIR-QUALITY MODELS -
623 EVALUATION OF THE EFFECTS OF LAYER THICKNESS AND VERTICAL PROFILE
624 CORRECTION ON SURFACE OZONE CONCENTRATIONS, *Atmospheric Environment*, 29,
625 105-126, [https://doi.org/10.1016/1352-2310\(94\)00225-a](https://doi.org/10.1016/1352-2310(94)00225-a), 1995.
- 626 Cao, X. H., Huo, S. L., Zhang, H. X., Zheng, J. Q., He, Z. S., Ma, C. Z., Song, S.: Source emissions and
627 climate change impacts on the multimedia transport and fate of persistent organic pollutants,
628 Chaohu watershed, eastern China, *Journal of Environmental Sciences*, 109, 15-25,
629 <https://doi.org/10.1016/j.jes.2021.02.028>, 2021.

630 Chen, H. S., Wang, Z. F., Li, J., Tang, X., Ge, B. Z., Wu, X. L., Wild, O., Carmichael, G. R.: GNAQPMS-
631 Hg v1.0, a global nested atmospheric mercury transport model: model description, evaluation
632 and application to trans-boundary transport of Chinese anthropogenic emissions, *Geoscientific*
633 *Model Development*, 8, 2857-2876, <https://doi.org/10.5194/gmd-8-2857-2015>, 2015.

634 Chen, S. C., Liao, C. M.: Health risk assessment on human exposed to environmental polycyclic aromatic
635 hydrocarbons pollution sources, *Science of the Total Environment*, 366, 112-123,
636 <https://doi.org/10.1016/j.scitotenv.2005.08.047>, 2006.

637 Chen, X. S., Wang, Z. F., Li, J., Yu, F. Q.: Development of a Regional Chemical Transport Model with
638 Size-Resolved Aerosol Microphysics and Its Application on Aerosol Number Concentration
639 Simulation over China, *Sola*, 10, 83-87, <https://doi.org/10.2151/sola.2014-017>, 2014.

640 Chen, X. S., Yu, F. Q., Yang, W. Y., Sun, Y. L., Chen, H. S., Du, W., Zhao, J., Wei, Y., Wei, L. F., Du, H.
641 Y., Wang, Z., Wu, Q. Z., Li, J., An, J. L., Wang, Z. F.: Global-regional nested simulation of
642 particle number concentration by combing microphysical processes with an evolving organic
643 aerosol module, *Atmospheric Chemistry and Physics*, 21, 9343-9366,
644 <https://doi.org/10.5194/acp-21-9343-2021>, 2021.

645 Crippa, M., Solazzo, E., Huang, G. L., Guizzardi, D., Koffi, E., Muntean, M., Schieberle, C., Friedrich,
646 R., Janssens-Maenhout, G.: High resolution temporal profiles in the Emissions Database for
647 Global Atmospheric Research, *Scientific Data*, 7, 17, [https://doi.org/10.1038/s41597-020-0462-](https://doi.org/10.1038/s41597-020-0462-2)
648 [2](https://doi.org/10.1038/s41597-020-0462-2), 2020.

649 Dachs, J., Eisenreich, S. J.: Adsorption onto aerosol soot carbon dominates gas-particle partitioning of
650 polycyclic aromatic hydrocarbons, *Environmental Science & Technology*, 34, 3690-3697,
651 <https://doi.org/10.1021/es991201+>, 2000.

652 **Ding, D., Xing, J., Wang, S.X., Liu, K.Y., Hao, J.M.: Estimated Contributions of Emissions**
653 **Controls, Meteorological Factors, Population Growth, and Changes in Baseline Mortality**
654 **to Reductions in Ambient PM_{2.5} and PM_{2.5}-Related Mortality in China, 2013-2017.**
655 ***Environmental Health Perspectives*, 127, 12, <https://doi.org/10.1289/ehp4157>, 2019.**

656 Dong, Z. S., Kong, Z. H., Dong, Z., Shang, L. Q., Zhang, R. Q., Xu, R. X., Li, X.: Air pollution prevention
657 in central China: Effects on particulate-bound PAHs from 2010 to 2018, *Journal of*
658 *Environmental Management*, 344, 11, <https://doi.org/10.1016/j.jenvman.2023.118555>, 2023.

659 Du, H. Y., Li, J., Chen, X. S., Wang, Z. F., Sun, Y. L., Fu, P. Q., Li, J. J., Gao, J., Wei, Y.: Modeling of
660 aerosol property evolution during winter haze episodes over a megacity cluster in northern
661 China: roles of regional transport and heterogeneous reactions of SO₂,
662 Atmospheric Chemistry and Physics, 19, 9351-9370, <https://doi.org/10.5194/acp-19-9351-2019>,
663 2019.

664 Efstathiou, C. I., Matejovičová, J., Bieser, J., Lammel, G.: Evaluation of gas-particle partitioning in a
665 regional air quality model for organic pollutants, Atmospheric Chemistry and Physics, 16,
666 15327-15345, <https://doi.org/10.5194/acp-16-15327-2016>, 2016.

667 Feng, Y. Y., Ning, M., Lei, Y., Sun, Y. M., Liu, W., Wang, J. N.: Defending blue sky in China:
668 Effectiveness of the "Air Pollution Prevention and Control Action Plan" on air quality
669 improvements from 2013 to 2017, Journal of Environmental Management, 252, 13,
670 <https://doi.org/10.1016/j.jenvman.2019.109603>, 2019.

671 Finlayson-Pitts, B. J., Pitts, J. N. Chemistry of the Upper and Lower Atmosphere: Theory, Experiments,
672 and Applications. 2000.

673 Friedman, C. L., Pierce, J. R., Selin, N. E.: Assessing the Influence of Secondary Organic versus Primary
674 Carbonaceous Aerosols on Long-Range Atmospheric Polycyclic Aromatic Hydrocarbon
675 Transport, Environmental Science & Technology, 48, 3293-3302,
676 <https://doi.org/10.1021/es405219r>, 2014.

677 Friedman, C. L., Selin, N. E.: Long-Range Atmospheric Transport of Polycyclic Aromatic Hydrocarbons:
678 A Global 3-D Model Analysis Including Evaluation of Arctic Sources, Environmental Science
679 & Technology, 46, 9501-9510, <https://doi.org/10.1021/es301904d>, 2012.

680 Galarneau, E., Makar, P. A., Zheng, Q., Narayan, J., Zhang, J., Moran, M. D., Bari, M. A., Pathela, S.,
681 Chen, A., Chlumsky, R.: PAH concentrations simulated with the AURAMS-PAH chemical
682 transport model over Canada and the USA, Atmospheric Chemistry and Physics, 14, 4065-4077,
683 <https://doi.org/10.5194/acp-14-4065-2014>, 2014.

684 Gusev, A., Ilyin, I., Rozovskaya, O., Shatalov, V., Travnikov, O., Strijkina I. Assessment of transboundary
685 pollution by toxic substances: Heavy metals and POPs, Meteorological Synthesizing Centre -
686 East, Russia, 74 pp., 2019.

687 Han, F. L., Guo, H., Hu, J. L., Zhang, J., Ying, Q., Zhang, H. L.: Sources and health risks of ambient

688 polycyclic aromatic hydrocarbons in China, *Science of the Total Environment*, 698, 13,
689 <https://doi.org/10.1016/j.scitotenv.2019.134229>, 2020.

690 Hansen, K. M., Christensen, J. H., Brandt, J., Frohn, L. M., Geels, C.: Modelling atmospheric transport
691 of α -hexachlorocyclohexane in the Northern Hemisphere with a 3-D dynamical model: DEHM-
692 POP, *Atmos. Chem. Phys.*, 4, 1125-1137, <https://doi.org/10.5194/acp-4-1125-2004>, 2004.

693 Haritash, A. K., Kaushik, C. P.: Biodegradation aspects of Polycyclic Aromatic Hydrocarbons (PAHs): A
694 review, *Journal of Hazardous Materials*, 169, 1-15,
695 <https://doi.org/10.1016/j.jhazmat.2009.03.137>, 2009.

696 Harner, T., Bidleman, T. F.: Octanol-air partition coefficient for describing particle/gas partitioning of
697 aromatic compounds in urban air, *Environmental Science & Technology*, 32, 1494-1502,
698 <https://doi.org/10.1021/es970890r>, 1998.

699 Inomata, Y., Kajino, M., Sato, K., Ohara, T., Kurokawa, J., Ueda, H., Tang, N., Hayakawa, K., Ohizumi,
700 T., Akimoto, H.: Source contribution analysis of surface particulate polycyclic aromatic
701 hydrocarbon concentrations in northeastern Asia by source-receptor relationships,
702 *Environmental Pollution*, 182, 324-334, <https://doi.org/10.1016/j.envpol.2013.07.020>, 2013.

703 Inomata, Y., Kajino, M., Sato, K., Ohara, T., Kurokawa, J. I., Ueda, H., Tang, N., Hayakawa, K., Ohizumi,
704 T., Akimoto, H.: Emission and Atmospheric Transport of Particulate PAHs in Northeast Asia,
705 *Environmental Science & Technology*, 46, 4941-4949, <https://doi.org/10.1021/es300391w>,
706 2012.

707 Jonker, M. T. O., Koelmans, A. A.: Sorption of polycyclic aromatic hydrocarbons and polychlorinated
708 biphenyls to soot and soot-like materials in the aqueous environment mechanistic considerations,
709 *Environmental Science & Technology*, 36, 3725-3734, <https://doi.org/10.1021/es020019x>, 2002.

710 Jury, W. A., Spencer, W. F., Farmer, W. J.: Behavior Assessment Model for Trace Organics in Soil: I.
711 Model Description, *Journal of Environmental Quality*, 12, 558-564,
712 <https://doi.org/10.2134/jeq1983.00472425001200040025x>, 1983.

713 Kahan, T. F., Kwamena, N. O. A., Donaldson, D. J.: Heterogeneous ozonation kinetics of polycyclic
714 aromatic hydrocarbons on organic films, *Atmospheric Environment*, 40, 3448-3459,
715 <https://doi.org/10.1016/j.atmosenv.2006.02.004>, 2006.

716 Karickhoff, S. W.: Semi-empirical estimation of sorption of hydrophobic pollutants on natural sediments

717 and soils, *Chemosphere*, 10, 833-846, [https://doi.org/10.1016/0045-6535\(81\)90083-7](https://doi.org/10.1016/0045-6535(81)90083-7), 1981.

718 Keyte, I. J., Harrison, R. M., Lammel, G.: Chemical reactivity and long-range transport potential of
719 polycyclic aromatic hydrocarbons - a review, *Chemical Society Reviews*, 42, 9333-9391,
720 <https://doi.org/10.1039/c3cs60147a>, 2013.

721 Klöpffer, W., Wagner, B., Scheringer, M.: Atmospheric degradation of organic substances data for
722 persistence and long-range transport potential, *Environmental Science and Pollution Research*
723 - International, 14, 143-144, <https://doi.org/10.1065/espr2007.04.408>, 2007.

724 Kwamena, N. O. A., Clarke, J. P., Kahan, T. F., Diamond, M. L., Donaldson, D. J.: Assessing the
725 importance of heterogeneous reactions of polycyclic aromatic hydrocarbons in the urban
726 atmosphere using the Multimedia Urban Model, *Atmospheric Environment*, 41, 37-50,
727 <https://doi.org/10.1016/j.atmosenv.2006.08.016>, 2007.

728 Lammel, G., Dvorská, A., Klánová, J., Kohoutek, J., Kukacka, P., Prokes, R., Sehili, A. M.: Long-range
729 Atmospheric Transport of Polycyclic Aromatic Hydrocarbons is Worldwide Problem - Results
730 from Measurements at Remote Sites and Modelling, *Acta Chimica Slovenica*, 62, 729-735, 2015.

731 Lammel, G., Sehili, A. M.: Global fate and distribution of polycyclic aromatic hydrocarbons emitted from
732 Europe and Russia, *Atmospheric Environment*, 41, 8301-8315,
733 <https://doi.org/10.1016/j.atmosenv.2007.06.050>, 2007.

734 Lammel, G., Sehili, A. M., Bond, T. C., Feichter, J., Grassl, H.: Gas/particle partitioning and global
735 distribution of polycyclic aromatic hydrocarbons--a modelling approach, *Chemosphere*, 76, 98-
736 106, <https://doi.org/10.1016/j.chemosphere.2009.02.017>, 2009.

737 Li, J., Wang, Z. F., Zhuang, G., Luo, G., Sun, Y., Wang, Q.: Mixing of Asian mineral dust with
738 anthropogenic pollutants over East Asia: a model case study of a super-duststorm in March 2010,
739 *Atmospheric Chemistry and Physics*, 12, 7591-7607, <https://doi.org/10.5194/acp-12-7591-2012>,
740 2012.

741 Li, R. F., Zhang, J., Krebs, P.: Global trade drives transboundary transfer of the health impacts of
742 polycyclic aromatic hydrocarbon emissions, *Communications Earth & Environment*, 3, 13,
743 <https://doi.org/10.1038/s43247-022-00500-y>, 2022.

744 Li, Z., Mulholland, J. A., Romanoff, L. C., Pittman, E. N., Trinidad, D. A., Lewin, M. D., Sjödin, A.:
745 Assessment of non-occupational exposure to polycyclic aromatic hydrocarbons through

746 personal air sampling and urinary biomonitoring, *Journal of Environmental Monitoring*, 12,
747 1110-1118, <https://doi.org/10.1039/c000689k>, 2010.

748 Lin, Y., Ma, Y. Q., Qiu, X. H., Li, R., Fang, Y. H., Wang, J. X., Zhu, Y. F., Hu, D.: Sources, transformation,
749 and health implications of PAHs and their nitrated, hydroxylated, and oxygenated derivatives in
750 PM_{2.5} in Beijing, *Journal of Geophysical Research-Atmospheres*, 120, 7219-7228,
751 <https://doi.org/10.1002/2015jd023628>, 2015.

752 **Lin, Y., Shi, X. D., Qiu, X. H., Jiang, X., Liu, J. M., Zhong, P. W., Ge, Y. H., Tseng, C.-H., Zhang, J.**
753 **F., Zhu, T., Araujo, J. A., Zhu, Y. F.: Reduction in polycyclic aromatic hydrocarbon**
754 **exposure in Beijing following China ' s clean air actions. *Science Bulletin*,**
755 **<https://doi.org/10.1016/j.scib.2024.08.015>, 2024.**

756 Liu, S. J., Lu, Y. L., Wang, T. Y., Xie, S. W., Jones, K. C., Sweetman, A. J.: Using gridded multimedia
757 model to simulate spatial fate of Benzo α pyrene on regional scale, *Environment International*,
758 63, 53-63, <https://doi.org/10.1016/j.envint.2013.10.015>, 2014.

759 Lou, S. J., Shrivastava, M., Ding, A. J., Easter, R. C., Fast, J. D., Rasch, P. J., Shen, H. Z., Simonich, S.
760 M., Smith, S. J., Tao, S., Zelenyuk, A.: Shift in Peaks of PAH-Associated Health Risks From
761 East Asia to South Asia and Africa in the Future, *Earths Future*, 11, 15,
762 <https://doi.org/10.1029/2022ef003185>, 2023.

763 Ma, W. L., Liu, L. Y., Jia, H. L., Yang, M., Li, Y. F.: PAHs in Chinese atmosphere Part I: Concentration,
764 source and temperature dependence, *Atmospheric Environment*, 173, 330-337,
765 <https://doi.org/10.1016/j.atmosenv.2017.11.029>, 2018.

766 Ma, W. L., Zhu, F. J., Liu, L. Y., Jia, H. L., Yang, M., Li, Y. F.: PAHs in Chinese atmosphere Part II: Health
767 risk assessment, *Ecotoxicology and Environmental Safety*, 200, 9,
768 <https://doi.org/10.1016/j.ecoenv.2020.110774>, 2020.

769 Mu, Q., Shiraiwa, M., Octaviani, M., Ma, N., Ding, A. J., Su, H., Lammel, G., Pöschl, U., Cheng, Y. F.:
770 Temperature effect on phase state and reactivity controls atmospheric multiphase chemistry and
771 transport of PAHs, *Science Advances*, 4, 8, <https://doi.org/10.1126/sciadv.aap7314>, 2018.

772 Nam, K. J., Li, Q., Heo, S. K., Tariq, S., Loy-Benitez, J., Woo, T. Y., Yoo, C. K.: Inter-regional multimedia
773 fate analysis of PAHs and potential risk assessment by integrating deep learning and climate
774 change scenarios, *Journal of Hazardous Materials*, 411, 12,

775 <https://doi.org/10.1016/j.jhazmat.2021.125149>, 2021.

776 Octaviani, M., Tost, H., Lammel, G.: Global simulation of semivolatile organic compounds - development
777 and evaluation of the MESSy submodel SVOC (v1.0), *Geoscientific Model Development*, 12,
778 3585-3607, <https://doi.org/10.5194/gmd-12-3585-2019>, 2019.

779 Odabasi, M., Cetin, E., Sofuoglu, A.: Determination of octanol–air partition coefficients and supercooled
780 liquid vapor pressures of PAHs as a function of temperature: Application to gas–particle
781 partitioning in an urban atmosphere, *Atmospheric Environment*, 40, 6615-6625,
782 <https://doi.org/10.1016/j.atmosenv.2006.05.051>, 2006.

783 Quan, J. N., Tie, X. X., Zhang, Q., Liu, Q., Li, X., Gao, Y., Zhao, D. L.: Characteristics of heavy aerosol
784 pollution during the 2012-2013 winter in Beijing, China, *Atmospheric Environment*, 88, 83-89,
785 <https://doi.org/10.1016/j.atmosenv.2014.01.058>, 2014.

786 Ravindra, K., Sokhi, R., Van Grieken, R.: Atmospheric polycyclic aromatic hydrocarbons: Source
787 attribution, emission factors and regulation, *Atmospheric Environment*, 42, 2895-2921,
788 <https://doi.org/10.1016/j.atmosenv.2007.12.010>, 2008.

789 San José, R., Pérez, J. L., Callén, M. S., López, J. M., Mastral, A.: BaP (PAH) air quality modelling
790 exercise over Zaragoza (Spain) using an adapted version of WRF-CMAQ model,
791 *Environmental Pollution*, 183, 151-158, <https://doi.org/10.1016/j.envpol.2013.02.025>, 2013.

792 Seigneur, C., Karamchandani, P., Lohman, K., Vijayaraghavan, K., Shia, R. L.: Multiscale modeling of
793 the atmospheric fate and transport of mercury, *Journal of Geophysical Research-Atmospheres*,
794 106, 27795-27809, <https://doi.org/10.1029/2000jd000273>, 2001.

795 Semeena, V. S., Lammel, G.: The significance of the grasshopper effect on the atmospheric distribution
796 of persistent organic substances, *Geophysical Research Letters*, 32, 5,
797 <https://doi.org/10.1029/2004gl022229>, 2005.

798 Shen, H. Z., Tao, S., Liu, J. F., Huang, Y., Chen, H., Li, W., Zhang, Y. Y., Chen, Y. C., Su, S., Lin, N., Xu,
799 Y. Y., Li, B. G., Wang, X. L., Liu, W. X.: Global lung cancer risk from PAH exposure highly
800 depends on emission sources and individual susceptibility, *Scientific Reports*, 4, 8,
801 <https://doi.org/10.1038/srep06561>, 2014.

802 Shrivastava, M., Lou, S., Zelenyuk, A., Easter, R. C., Corley, R. A., Thrall, B. D., Rasch, P. J., Fast, J. D.,
803 Simonich, S. L. M., Shen, H. Z., Tao, S.: Global long-range transport and lung cancer risk from

804 polycyclic aromatic hydrocarbons shielded by coatings of organic aerosol, Proceedings of the
805 National Academy of Sciences of the United States of America, 114, 1246-1251,
806 <https://doi.org/10.1073/pnas.1618475114>, 2017.

807 Skamarock, W. C., Klemp, J. B., Dudhia, J., Gill, D., Barker, D. M., Duda, M. G., Huang, X.-Y., Wang,
808 W., Powers, J. G. A Description of the Advanced Research WRF Version 3. 2008.

809 Smith, R. L., Davis, J. M., Speckman, P.: Assessing the human health risk of atmospheric particles,
810 Novartis Found Symp, 220, 59-72; discussion 72-9,
811 <https://doi.org/10.1002/9780470515600.ch4>, 1999.

812 Stockwell, W. R., Middleton, P., Chang, J. S., Tang, X. Y.: The Second Generation Regional Acid
813 Deposition Model Chemical Mechanism for Regional Air Quality Modeling, Journal of
814 Geophysical Research-Atmospheres, 95, 16343-16367,
815 <https://doi.org/10.1029/JD095iD10p16343>, 1990.

816 Strand, A., Hov, O.: A model strategy for the simulation of chlorinated hydrocarbon distributions in the
817 global environment, Water Air and Soil Pollution, 86, 283-316,
818 <https://doi.org/10.1007/bf00279163>, 1996.

819 Su, C., Zheng, D. F., Zhang, H., Liang, R. Y.: The past 40 years' assessment of urban-rural differences in
820 Benzo a pyrene contamination and human health risk in coastal China, Science of the Total
821 Environment, 901, 9, <https://doi.org/10.1016/j.scitotenv.2023.165993>, 2023.

822 van Noort, P. C. M.: A thermodynamics-based estimation model for adsorption of organic compounds by
823 carbonaceous materials in environmental sorbents, Environmental Toxicology and Chemistry,
824 22, 1179-1188, 2003.

825 Walcek, C. J., Aleksic, N. M.: A simple but accurate mass conservative, peak-preserving, mixing ratio
826 bounded advection algorithm with Fortran code, Atmospheric Environment, 32, 3863-3880,
827 [https://doi.org/10.1016/s1352-2310\(98\)00099-5](https://doi.org/10.1016/s1352-2310(98)00099-5), 1998.

828 Wang, L., Zhang, F. Y., Pilot, E., Yu, J., Nie, C. J., Holdaway, J., Yang, L. S., Li, Y. H., Wang, W. Y.,
829 Vardoulakis, S., Krafft, T.: Taking Action on Air Pollution Control in the Beijing-Tianjin-Hebei
830 (BTH) Region: Progress, Challenges and Opportunities, International Journal of Environmental
831 Research and Public Health, 15, 27, <https://doi.org/10.3390/ijerph15020306>, 2018.

832 Wang, Y. S., Li, W. J., Gao, W. K., Liu, Z. R., Tian, S. L., Shen, R. R., Ji, D. S., Wang, S., Wang, L. L.,

833 Tang, G. Q., Song, T., Cheng, M. T., Wang, G. H., Gong, Z. Y., Hao, J. M.,Zhang, Y. H.: Trends
834 in particulate matter and its chemical compositions in China from 2013-2017, Science China-
835 Earth Sciences, 62, 1857-1871, <https://doi.org/10.1007/s11430-018-9373-1>, 2019.

836 Wang, Z. F., Maeda, T., Hayashi, M., Hsiao, L. F.,Liu, K. Y.: A nested air quality prediction modeling
837 system for urban and regional scales: Application for high-ozone episode in Taiwan, Water Air
838 and Soil Pollution, 130, 391-396, <https://doi.org/10.1023/a:1013833217916>, 2001.

839 Wang, Z. X., Li, J. X., Mu, X., Zhao, L. Y., Gu, C., Gao, H., Ma, J. M., Mao, X. X.,Huang, T.: A WRF-
840 CMAQ modeling of atmospheric PAH cycling and health risks in the heavy petrochemical
841 industrialized Lanzhou valley, Northwest China, Journal of Cleaner Production, 291, 9,
842 <https://doi.org/10.1016/j.jclepro.2021.125989>, 2021.

843 Wei, Y., Chen, X. S., Chen, H. S., Li, J., Wang, Z. F., Yang, W. Y., Ge, B. Z., Du, H. Y., Hao, J. Q., Wang,
844 W., Li, J. J., Sun, Y. L.,Huang, H. L.: IAP-AACM v1.0: a global to regional evaluation of the
845 atmospheric chemistry model in CAS-ESM, Atmospheric Chemistry and Physics, 19, 8269-
846 8296, <https://doi.org/10.5194/acp-19-8269-2019>, 2019.

847 Wu, Z. C., Chen, X. S., and Wang, Z. F.: A Global-Regional Nested Model of Polycyclic aromatic
848 hydrocarbons, Zenodo [code], <https://doi.org/10.5281/zenodo.12214119>, 2024.

849 Wu, Z. C., Chen, X. S., and Wang, Z. F.: Results and validation of Global-Regional Nested Model for
850 polycyclic aromatic hydrocarbons., Zenodo [data set],
851 <https://doi.org/10.5281/zenodo.11595165>, 2024.

852 Yan, D. H., Wu, S. H., Zhou, S. L., Tong, G. J., Li, F. F., Wang, Y. M.,Li, B. J.: Characteristics, sources
853 and health risk assessment of airborne particulate PAHs in Chinese cities: A review,
854 Environmental Pollution, 248, 804-814, <https://doi.org/10.1016/j.envpol.2019.02.068>, 2019.

855 **Yang, L., Zhang, X., Xing, W.L., Zhou, Q.Y., Zhang, L.L., Wu, Q., Zhou, Z.J., Chen, R.J., Toriba,**
856 **A., Hayakawa, K., Tang, N.: Yearly variation in characteristics and health risk of**
857 **polycyclic aromatic hydrocarbons and nitro-PAHs in urban shanghai from 2010-2018.**
858 **Journal of Environmental Sciences, 99, 72-79, <https://doi.org/10.1016/j.jes.2020.06.017>,**
859 **2021.**

860 Ye, Q., Li, J., Chen, X., Chen, H., Yang, W., Du, H., Pan, X., Tang, X., Wang, W., Zhu, L., Li, J., Wang,
861 Z.,Wang, Z.: High-resolution modeling of the distribution of surface air pollutants and their

862 intercontinental transport by a global tropospheric atmospheric chemistry source–receptor
863 model (GNAQPMS-SM), *Geoscientific Model Development*, 14, 7573-7604,
864 <https://doi.org/10.5194/gmd-14-7573-2021>, 2021.

865 Zaveri, R. A., Peters, L. K.: A new lumped structure photochemical mechanism for large-scale
866 applications, *Journal of Geophysical Research-Atmospheres*, 104, 30387-30415,
867 <https://doi.org/10.1029/1999jd900876>, 1999.

868 **Zhang, H., Zhang, X., Wang, Y., Bai, P.C., Zhang, L.L., Chen, L.J., Han, C., Yang, W.J., Wang,**
869 **Q.M., Cai, Y.P., Nagao, S., Tang, N.: Factor analysis of recent variations of atmospheric**
870 **polycyclic aromatic hydrocarbons (PAHs) and 1-nitropyrene (1-NP) in Shenyang, China**
871 **from 2014 to 2020. *Atmospheric Pollution Research*, 14, 8,**
872 **<https://doi.org/10.1016/j.apr.2023.101900>, 2023.**

873 **Zhang, J.W., Feng, L.H., Zhao, Y., Hou, C.C., Gu, Q.: Health risks of PM2.5-bound polycyclic**
874 **aromatic hydrocarbon (PAH) and heavy metals (PPAH&HM) during the replacement of**
875 **central heating with urban natural gas in Tianjin, China. *Environ. Geochem. Health*, 44,**
876 **2495-2514, <https://doi.org/10.1007/s10653-021-01040-8>, 2022.**

877 Zhang, L., Brook, J. R., Vet, R.: A revised parameterization for gaseous dry deposition in air-quality
878 models, *Atmospheric Chemistry and Physics*, 3, 2067-2082, [https://doi.org/10.5194/acp-3-](https://doi.org/10.5194/acp-3-2067-2003)
879 [2067-2003](https://doi.org/10.5194/acp-3-2067-2003), 2003.

880 Zhang, M., Xie, J. F., Wang, Z. T., Zhao, L. J., Zhang, H., Li, M.: Determination and source identification
881 of priority polycyclic aromatic hydrocarbons in PM2.5 in Taiyuan, China, *Atmospheric*
882 *Research*, 178, 401-414, <https://doi.org/10.1016/j.atmosres.2016.04.005>, 2016.

883 Zhang, Q., Zheng, Y. X., Tong, D., Shao, M., Wang, S. X., Zhang, Y. H., Xu, X. D., Wang, J. N., He, H.,
884 Liu, W. Q., Ding, Y. H., Lei, Y., Li, J. H., Wang, Z. F., Zhang, X. Y., Wang, Y. S., Cheng, J., Liu,
885 Y., Shi, Q. R., Yan, L., Geng, G. N., Hong, C. P., Li, M., Liu, F., Zheng, B., Cao, J. J., Ding, A.
886 J., Gao, J., Fu, Q. Y., Huo, J. T., Liu, B. X., Liu, Z. R., Yang, F. M., He, K. B., Hao, J. M.: Drivers
887 of improved PM2.5 air quality in China from 2013 to 2017, *Proceedings of the National*
888 *Academy of Sciences of the United States of America*, 116, 24463-24469,
889 <https://doi.org/10.1073/pnas.1907956116>, 2019.

890 Zhang, Y., Hemperly, J., Meskhidze, N., Skamarock, W. C.: The Global Weather Research and

891 Forecasting (GWRP) Model: Model Evaluation, Sensitivity Study, and Future Year Simulation,
892 Atmospheric and Climate Sciences, 2, 231-253, <https://doi.org/10.4236/acs.2012.23024>, 2012a.

893 Zhang, Y., Jaeglé, L., van Donkelaar, A., Martin, R. V., Holmes, C. D., Amos, H. M., Wang, Q., Talbot,
894 R., Artz, R., Brooks, S., Luke, W., Holsen, T. M., Felton, D., Miller, E. K., Perry, K. D., Schmeltz,
895 D., Steffen, A., Tordon, R., Weiss-Penzias, P., Zsolway, R.: Nested-grid simulation of mercury
896 over North America, Atmospheric Chemistry and Physics, 12, 6095-6111,
897 <https://doi.org/10.5194/acp-12-6095-2012>, 2012b.

898 Zhang, Y., Shen, H., Tao, S., Ma, J.: Modeling the atmospheric transport and outflow of polycyclic
899 aromatic hydrocarbons emitted from China, Atmospheric Environment, 45, 2820-2827,
900 <https://doi.org/10.1016/j.atmosenv.2011.03.006>, 2011a.

901 Zhang, Y., Tao, S., Ma, J., Simonich, S.: Transpacific transport of benzo[a]pyrene emitted from Asia,
902 Atmospheric Chemistry and Physics, 11, 11993-12006, [https://doi.org/10.5194/acp-11-11993-](https://doi.org/10.5194/acp-11-11993-2011)
903 2011, 2011b.

904 Zhang, Y. X., Tao, S.: Global atmospheric emission inventory of polycyclic aromatic hydrocarbons (PAHs)
905 for 2004, Atmospheric Environment, 43, 812-819,
906 <https://doi.org/10.1016/j.atmosenv.2008.10.050>, 2009.

907 Zhang, Y. X., Tao, S., Shen, H. Z., Ma, J. M.: Inhalation exposure to ambient polycyclic aromatic
908 hydrocarbons and lung cancer risk of Chinese population, Proceedings of the National Academy
909 of Sciences of the United States of America, 106, 21063-21067,
910 <https://doi.org/10.1073/pnas.0905756106>, 2009.

911 Zhen, Z. X.: Observation and simulation of atmospheric polycyclic aromatic hydrocarbons in the North
912 China Plain, Ph.D.thesis, Nanjing university of information science and technology, China, 142
913 pp., 2023.

914 Zhu, F. J., Ma, W. L., Hu, P. T., Zhang, Z. F., Li, Y. F.: Temporal trends of atmospheric PAHs: Implications
915 for the influence of the clean air action, Journal of Cleaner Production, 296, 8,
916 <https://doi.org/10.1016/j.jclepro.2021.126494>, 2021.